

GUTZWILLER-CORRELATED WAVE FUNCTIONS: APPLICATION TO FERROMAGNETIC NICKEL

Jörg Bünemann¹, Florian Gebhard¹, Torsten Ohm², Stefan Weiser², and Werner Weber²

¹ Fachbereich Physik and Material Sciences Center,
Philipps-Universität Marburg, D-35032 Marburg, Germany

² Institut für Physik,
Universität Dortmund, D-44221 Dortmund, Germany

1 Introduction

1.1 Ferromagnetism: whither theory?

Metallic ferromagnetism has since long been a controversial subject in solid-state theory. From early on, two schools of thought have been competing. The first, based on ideas of Slater, Stoner, and Wohlfarth, turns to the band aspects of metallic ferromagnets such as iron, cobalt, and nickel [1]. The itineracy of the conduction electrons, including those of the open $3d$ shell, is considered to dominate the electron-electron interaction. The second school, going back to van-Vleck [2] and Gutzwiller [3], stresses the localized character of the $3d$ electrons in transition metals and their compounds; local magnetic moments are indeed manifest in magnetic insulators which are often oxides and halides of transition metals. In the van-Vleck–Gutzwiller school, local moments are seen as an important source of magnetism, common to both ferromagnetic transition metals and their insulating compounds. Therefore, the van-Vleck–Gutzwiller school emphasizes the importance of correlations as a consequence of the electron-electron interactions.

As the Slater–Stoner–Wohlfarth school considers electronic correlations to be of minor importance, it treats the electron–electron interaction in simple approximations such as Hartree–Fock theory, see [1]. Later, the density–functional theory (DFT) in its spin–dependent versions (SDFT) took over the role of Hartree–Fock or x_α schemes of the Slater school. For more than two decades, SDFT energy–band calculations by various groups have provided reasonably accurate results for quite a number of properties of metallic ferromagnets, e.g., magnetic moments and the overall shape of the Fermi surface. An early problem was the observation that SDFT in standard local–density approximation (LDA) does not give the bcc lattice as the most stable crystal structure for iron, instead fcc Fe is found to be stable. This problem was overcome by the introduction of generalized gradient expansions (GGA) of the density [4].

Until recently the van–Vleck–Gutzwiller school could not provide much more than intuitive arguments for its case because ferromagnetism is seen as a genuine, difficult many–body problem. For decades, only simplistic models could be treated with some reliability, e.g., the one–band Hubbard model, which, however, exhibits ferromagnetism only for an extremely large Hubbard interaction or a pathological density of state [5]. In the past, despite some partial successes [6], correlated–electron theory could not describe real materials in much detail. Over the last decade new theoretical tools have been developed which try to combine the merits of density–functional theory with those of advanced many–body approaches, e.g., the LDA–*GW* approximation [7]. A general problem of correlated–electron theories is the construction of suitable model Hamiltonians. Progress in this direction has been made recently, e.g., the ‘down–folding’ scheme permits a systematic construction of Hamiltonians in a reduced Hilbert space [8]. The one–particle dynamics of models for correlated lattice electrons can be determined, in principle, within the dynamical mean–field theory (DMFT) [9, 10, 11] which becomes exact in the limit of an infinite number of nearest neighbors (coordination number $Z \rightarrow \infty$). The ‘static approximation’ to DMFT is the ‘LDA+ U ’ scheme which has been applied to a variety of correlated–electron systems [12, 13, 14]. Moreover, DMFT has been extended in various ways, e.g., a combination of the LDA–*GW* approximation and the DMFT has been put forward [15]. Therefore, correlated–electron theories seem to approach a level of quality where a faithful comparison with experiments becomes possible.

In our group, we have extended the original Gutzwiller variational scheme to the full multi–band problem. Our theory provides total energies and magnetic moments of competing magnetic and non–magnetic phases and the single–particle excitation energies within Fermi–liquid theory. Thereby, our theory describes the dispersion of the conduction and valence bands and the Fermi surface as accessible, e.g., by angle–resolved photo–emission spectroscopy (ARPES), and the predictions of our Gutzwiller correlated–electron theory can be tested against experiments on transition metals and its compounds.

1.2 The nickel problem

In this article we address ferromagnetic nickel as the prototype of band ferromagnetic materials. On the experimental side, one of the reasons why nickel has been in the focus of interest, much more than iron or cobalt, is the relative ease to grow large single crystals.

Consequently, a lot of experimental investigations have been carried out on nickel in order to determine its magnetic properties and electronic structure. For a review, we refer to the articles [1, 16, 17, 18].

On the theoretical side, of all the iron group magnetic metals nickel is the most celebrated case of discrepancies between SDFT predictions and experimental results. Early on, de-Haas–van-Alphen data indicated the presence of only one hole ellipsoid in the Fermi surface of the minority spin bands, located around the X -point of the Brillouin zone [19]. In contrast, energy band calculations using SDFT predict two hole ellipsoids around the X -point, the X_5 -state of pure $d(t_{2g})$ orbital character, and the X_2 -state of pure $d(e_g)$ orbital character. Concomitantly, neutron scattering experiments [20] revealed that the orbital character of the nickel magnetic moment exhibits less e_g admixture than predicted by energy band calculations.

ARPES measurements confirmed the de-Haas–van-Alphen results: the minority X_2 -state of pure $d(e_g)$ orbital character was found to lie slightly below the Fermi level. Furthermore, the photoemission data differ considerably from SDFT over the whole range of occupied $3d$ bands. Most importantly, the width of the occupied part of the $3d$ bands is approximately $W = 3.3$ eV [21, 22], whereas SDFT gives $W_{\text{SDFT}} = 4.5$ eV, or larger [23]. ARPES studies also reveal big discrepancies between SDFT and experiment in the exchange splittings of majority and minority spin bands near the Fermi energy. The SDFT results give a rather isotropic exchange splitting of about 650 meV to 750 meV, whereas photoemission data show small and highly anisotropic exchange splittings between 160 meV for pure $3d(e_g)$ -states such as X_2 and 330 meV for pure $3d(t_{2g})$ -states such as S_3 near the X -point.

Another discrepancy concerns the position of the $L_{2'}$ -state. Experimentally, it is found approximately 1 eV below the Fermi energy E_F whereas the SDFT puts it to about 0.3 eV below E_F . This state is special as it represents the most binding, pure $4p$ -state [24]. An incorrect $4p$ -level implies that DFT slightly underestimates the partial density of the $4p$ electrons and, thus, the $3d$ -hole density.

Lastly, the size and the direction of the magnetic moment pose a big problem to SDFT. Early experiments using ferromagnetic electron resonance and the Einstein–de-Haas effect have produced the values $g = 2.183$ and $g' = 1.835$ which result in an orbital moment of $\mu_{\text{orb}} = 0.0507\mu_B$ per atom for nickel [1]. In general, the values of the orbital part of the magnetic moments in band ferromagnets are not very well reproduced in SDFT. Iron and cobalt show large deviations [25], even in relativistic SDFT calculations [26]. Moreover, the magneto-crystalline anisotropy energies are not correct, i.e., they come with the wrong sign in SDFT. As shown by Aubert and Gersdorf [27, 28], the value of the dominant anisotropy constant is $K_1 = -8.8 \mu\text{eV}$, i.e., the (111) direction is the easy axis in nickel. For a (001) magnetic moment, the energy is higher with an energy difference $E_{\text{aniso}} \equiv E_{111} - E_{001} \approx -3 \mu\text{eV}$ per atom. In contrast, it is $E_{\text{aniso}} > 0$ in SDFT calculations, e.g., by Daalderoop [26] so that $K_1 > 0$. The SDFT results for cobalt and iron are equally disappointing. At low temperatures, the complex behavior of the magnetic anisotropy as a function of temperature and the magnetic field was interpreted by Gersdorf [27] to be caused by a shift of the electronic state (001) $X_{2\downarrow}$ to about 3 meV above the Fermi energy. The famous second hole ellipsoid around the $X_{2\downarrow}$ indeed exists [27] as long as the

magnetic moment has an angle of less than 18 degrees with the (001) direction. However, the states (100) $X_{2\downarrow}$ and (010) $X_{2\downarrow}$ remain below E_F , about 33 meV [27].

All these discrepancies could not be overcome by SDFT modifications such as the GGA variants [4]. Apparently, a substantial improvement of SDFT results for nickel along these lines is presently not within reach. Recent correlated-electron theories remove the SDFT shortcomings only partially. For example, with LDA+ U -type calculations it seems to be possible to adjust to experiment the orbital moment, the magnetic anisotropy, and the Fermi surface topology [13, 14]; however, other quantities, especially the entire quasi-particle band structure, remain elusive within these correlated-electron theories.

1.3 Scope of this work

In this article we show that our Gutzwiller theory resolves all of the discrepancies described in Section 1.2. Gutzwiller theory reproduces the experimental Fermi surface topology, the quasi-particle band structure with the correct width and the anisotropic exchange splittings, and the magnetic anisotropy. This success for nickel corroborates the early views by van-Vleck and Gutzwiller: the inclusion of the electron-electron interaction on a many-body level is essential for a proper understanding of itinerant ferromagnetism.

We structure our article as follows. In Section 2 we introduce our general Gutzwiller-correlated wave functions for multi-band Hubbard models. In Section 3 we present analytical results in the limit of infinite coordination number which we apply to nickel. The remaining Sections 4–7 are devoted to an improved, concise derivation of our theory. A short outlook closes our presentation.

The class of variational wave functions for which our formulae apply goes much beyond our previous investigations [29, 30, 31]. First, the Gutzwiller correlator now employs projections onto eigenstates of an effective atomic Hamiltonian which makes the variational Hilbert space much more flexible with respect to local correlations. Second, our variational states cover the case of superconductivity in correlated multi-band lattice systems. For ferromagnetic nickel, it does not seem to be necessary to exploit fully these new flexibilities. Therefore, we restrain ourselves to the normal-conducting state.

2 Gutzwiller variational theory

In this section we first define Gutzwiller variational wave functions for multi-band Hubbard models. In the limit of infinite coordination number, $Z \rightarrow \infty$, the expectation value of the Hamiltonian can be written in terms of an effective single-particle Hamiltonian. We use this expression as an approximation in our numerical studies on fcc nickel ($Z = 12$).

2.1 Definitions

2.1.1 Gutzwiller-correlated wave functions

We consider the Gutzwiller-correlated wave functions

$$|\Psi_G\rangle \equiv \hat{P}_G |\Psi_0\rangle . \quad (1)$$

Here, $|\Psi_0\rangle$ is a normalized quasi-particle vacuum so that we may later apply Wick's theorem. Expectation values in $|\Psi_0\rangle$ are denoted by

$$\langle \hat{A} \rangle_0 \equiv \langle \Psi_0 | \hat{A} | \Psi_0 \rangle . \quad (2)$$

Expectation values in $|\Psi_G\rangle$ are denoted by

$$\langle \hat{A} \rangle_G \equiv \frac{\langle \Psi_G | \hat{A} | \Psi_G \rangle}{\langle \Psi_G | \Psi_G \rangle} . \quad (3)$$

The Gutzwiller correlator is a product of local correlators,

$$\hat{P}_G \equiv \prod_{\mathbf{m}} \hat{P}_{G|\mathbf{m}} , \quad (4)$$

which induce transitions between atomic configurations on lattice site \mathbf{m} ,

$$\hat{P}_{G|\mathbf{m}} \equiv \sum_{I_1, I_2} \lambda_{I_1, I_2|\mathbf{m}} |I_1\rangle_{\mathbf{m}\mathbf{m}} \langle I_2| . \quad (5)$$

Atomic configurations with at least one electron are defined by

$$|I\rangle_{\mathbf{m}} \equiv \prod_{\sigma \in I} \hat{c}_{\mathbf{m}, \sigma}^+ |\text{vacuum}\rangle_{\mathbf{m}} . \quad (6)$$

The operator $\hat{c}_{\mathbf{m}, \sigma}^+$ ($\hat{c}_{\mathbf{m}, \sigma}$) creates (annihilates) an electron on lattice site \mathbf{m} in the local spin-orbitals $\sigma = 1, 2, \dots, (2N_o)$ ($N_o = 1, 3, 5$ for s, p, d electrons). The sets I comprise all possible atomic occupancies with $|I| = 1, 2, \dots, (2N_o)$ electrons. $I = (\emptyset), (\sigma_1), (\sigma_1, \sigma_2), \dots, (\sigma_1, \dots, \sigma_{2N_o})$ denotes configurations with no, one, two, $\dots, 2N_o$ electrons. A fixed order among the orbitals is assumed, i.e., we have $\sigma_1 < \sigma_2 < \dots < \sigma_{2N_o}$ in the definition of the sets I . For example, there is only one configuration $(2N_o) \equiv (\sigma_1, \dots, \sigma_{2N_o}) = (1, \dots, 2N_o)$ which represents a fully occupied atom. All standard set operations are defined for the sets I , e.g., $I = I_1 \cup I_2$ is the set union, and $I = I_1 \setminus I_2$ denotes the set of elements in I_1 which are not in I_2 . We define the complement of I as $\bar{I} \equiv (2N_o) \setminus I$. Altogether there are $D_{\text{at}} = 2^{2N_o}$ atomic configurations, $D_{\text{at}} = 4, 64, 1024$ for s, p, d electrons.

We demand that $|I_1| + |I_2|$ is even in (5). This restriction permits pairing correlations with an even number of Fermions as in BCS theory. Furthermore, we address only Hermitian Gutzwiller correlators, $\hat{P}_{G|\mathbf{m}} = \hat{P}_{G|\mathbf{m}}^+$. Consequently, we demand

$$\lambda_{I_1, I_2|\mathbf{m}} = \lambda_{I_2, I_1|\mathbf{m}}^* . \quad (7)$$

Therefore, we can find atomic states $|\Gamma\rangle_{\mathbf{m}}$ such that

$$\hat{P}_{G|\mathbf{m}} = \sum_{\Gamma} \lambda_{\Gamma|\mathbf{m}} \hat{m}_{\Gamma|\mathbf{m}} \quad (8)$$

with real parameters $\lambda_{\Gamma|\mathbf{m}}$. Here,

$$\hat{m}_{\Gamma|\mathbf{m}} = |\Gamma\rangle_{\mathbf{m}\mathbf{m}} \langle \Gamma| \quad (9)$$

is the projection operator onto the state $|\Gamma\rangle_{\mathbf{m}}$. In terms of atomic configurations we have

$$|\Gamma\rangle_{\mathbf{m}} = \sum_I A_{I,\Gamma|\mathbf{m}} |I\rangle_{\mathbf{m}} \quad , \quad |I\rangle_{\mathbf{m}} = \sum_{\Gamma} A_{I,\Gamma|\mathbf{m}}^* |\Gamma\rangle_{\mathbf{m}} \quad (10)$$

where the unitary matrix $\tilde{A}_{\mathbf{m}}$ diagonalizes the matrix $\tilde{\lambda}_{\mathbf{m}}$,

$$\lambda_{\Gamma_1|\mathbf{m}} \delta_{\Gamma_1,\Gamma_2} = \sum_{I_1,I_2} A_{I_1,\Gamma_1|\mathbf{m}}^* \lambda_{I_1,I_2|\mathbf{m}} A_{I_2,\Gamma_2|\mathbf{m}} \quad (11)$$

In general, the state $|\Gamma\rangle_{\mathbf{m}}$ can be chosen as the eigenstates of some *effective* local atomic Hamiltonian $\hat{H}_{\text{at}}^{\text{eff}}$.

2.1.2 Multi-band Hubbard models

In this work we focus on ferromagnetism of transition metals. Therefore, we study the multi-band Hubbard model for N electrons on L lattice sites,

$$\hat{H} = \hat{T} + \hat{H}_{\text{at}} \quad (12)$$

with

$$\hat{T} = \sum_{\mathbf{i},\mathbf{j},\sigma\sigma'} t_{\mathbf{i},\mathbf{j}}^{\sigma\sigma'} \hat{c}_{\mathbf{i},\sigma}^+ \hat{c}_{\mathbf{j},\sigma'} = \sum_{\mathbf{k};\sigma\sigma'} \epsilon_{\sigma\sigma'}^0(\mathbf{k}) \hat{c}_{\mathbf{k},\sigma}^+ \hat{c}_{\mathbf{k},\sigma'} \quad (13)$$

$$\epsilon_{\sigma\sigma'}^0(\mathbf{k}) \equiv \frac{1}{L} \sum_{\mathbf{i},\mathbf{j}} e^{-i\mathbf{k}(\mathbf{j}-\mathbf{i})} t_{\mathbf{i},\mathbf{j}}^{\sigma\sigma'} \quad (14)$$

where we used translational invariance, $t_{\mathbf{i},\mathbf{j}}^{\sigma\sigma'} \equiv t^{\sigma\sigma'}(\mathbf{i}-\mathbf{j})$ to introduce the bare energy-band matrix elements $\epsilon_{\sigma\sigma'}^0(\mathbf{k})$. Note that we set $t_{\mathbf{i},\mathbf{i}}^{\sigma\sigma'} = 0$, i.e., the kinetic energy operator does not include the local potential terms $\epsilon_{\mathbf{i},\sigma\sigma'} \equiv \epsilon_{\sigma\sigma'}$ (e.g., exchange splittings, spin-orbit interaction) which are contained in the general, purely local Hamiltonian

$$\hat{H}_{\text{at}} = \sum_{\mathbf{m}} \sum_{I_1,I_2} U_{I_1,I_2|\mathbf{m}} |I_1\rangle_{\mathbf{m}\mathbf{m}} \langle I_2| = \sum_{\mathbf{m}} \sum_{\bar{\Gamma}} E_{\bar{\Gamma}|\mathbf{m}} \hat{m}_{\bar{\Gamma}|\mathbf{m}} \quad (15)$$

The projector onto the atomic eigenstate $|\bar{\Gamma}\rangle_{\mathbf{m}}$ on site \mathbf{m} is denoted $\hat{m}_{\bar{\Gamma}|\mathbf{m}}$. The unitary matrix $\tilde{B}_{\mathbf{m}}$ diagonalizes the matrix $\tilde{U}_{\mathbf{m}}$,

$$E_{\bar{\Gamma}_1|\mathbf{m}} \delta_{\bar{\Gamma}_1,\bar{\Gamma}_2} = \sum_{I_1,I_2} B_{I_1,\bar{\Gamma}_1|\mathbf{m}}^* U_{I_1,I_2|\mathbf{m}} B_{I_2,\bar{\Gamma}_2|\mathbf{m}} \quad (16)$$

For translation invariance, we have $E_{\bar{\Gamma}|\mathbf{m}} \equiv E_{\bar{\Gamma}}$, $U_{I_1,I_2|\mathbf{m}} \equiv U_{I_1,I_2}$, $\lambda_{I_1,I_2|\mathbf{m}} \equiv \lambda_{I_1,I_2}$, and $\lambda_{\Gamma|\mathbf{m}} \equiv \lambda_{\Gamma}$. Note that the eigenstates $|\bar{\Gamma}\rangle_{\mathbf{m}}$ of \hat{H}_{at} need not be identical to $|\Gamma\rangle_{\mathbf{m}}$. Therefore, the number of parameters λ_{I_1,I_2} in our general definition of the Gutzwiller correlator (5) is of the order of D_{at}^2 [= $\mathcal{O}(10^6)$ for d electrons]. In most practical applications, it is impossible to scan such a large variational space numerically. Therefore, one has to work with eigenstates $|\Gamma\rangle_{\mathbf{m}}$ of some *effective* atomic Hamiltonian $\hat{H}_{\text{at}}^{\text{eff}}$ which is characterized by a few physically motivated parameters. In this way, the numerical problem basically

reduces to the minimization of the ground-state energy with respect to the real variational parameters λ_Γ . This minimization problem is numerically tractable because the number of variational parameters is now reduced to the dimension of the atomic Hilbert space, $D_{\text{at}} = \mathcal{O}(10^3)$ for d electrons.

The values for the electron-transfer parameters $t_{i,j}^{\sigma\sigma'}$ and the correlation parameters U_{I_1, I_2} (or, equivalently, for $\epsilon_{\sigma\sigma'}^0(\mathbf{k})$ and $E_{\bar{\Gamma}}$) depend on the specific material under investigation. We shall specify them for nickel in Section 3.

2.2 Effective single-particle Hamiltonian for nickel

For our studies on nickel we simplify the calculations by working with the correlator

$$\hat{P}_{\mathbf{G}|\mathbf{m}} = \sum_{\Gamma} \lambda_{\Gamma} \hat{m}_{\Gamma|\mathbf{m}} \quad (17)$$

in which we choose the states $|\Gamma\rangle_{\mathbf{m}}$ to be identical to the eigenstates of the atomic Hamiltonian in (15), $|\Gamma\rangle_{\mathbf{m}} \equiv |\bar{\Gamma}\rangle_{\mathbf{m}}$. Therefore, our main numerical problem is the minimization of the variational energy with respect to the parameters λ_{Γ} .

In order to determine the variational ground state of \hat{H} one first needs to calculate the expectation value

$$\langle \hat{H} \rangle_{\mathbf{G}} = E^{\text{var}}(\{\lambda_{\Gamma}\}, \{|\Psi_0\rangle\}) \quad (18)$$

of the Hamiltonian \hat{H} as a function of the variational parameters λ_{Γ} and the one-particle wave-function $|\Psi_0\rangle$. In the limit of infinite spatial dimensions the expectation value of the local Hamiltonian (15) becomes

$$E^{\text{at}}(\{m_{\Gamma}\}) = L \sum_{\Gamma} E_{\Gamma} m_{\Gamma} . \quad (19)$$

The probability for finding the atomic state $|\Gamma\rangle_{\mathbf{m}}$,

$$m_{\Gamma} \equiv \langle \hat{m}_{\Gamma|\mathbf{m}} \rangle_{\mathbf{G}} = \lambda_{\Gamma}^2 \langle \hat{m}_{\Gamma|\mathbf{m}} \rangle_0 , \quad (20)$$

may be used to replace the original variational parameters λ_{Γ} because $\langle \hat{m}_{\Gamma|\mathbf{m}} \rangle_0$ is a simple function of the local density-matrix for the non-interacting system,

$$C_{\sigma\sigma'} = \langle \hat{c}_{\mathbf{m},\sigma}^+ \hat{c}_{\mathbf{m},\sigma'} \rangle_0 . \quad (21)$$

The one-particle product state $|\Psi_0\rangle$ is the ground state of the effective single-particle Hamiltonian

$$\hat{T}^{\text{eff}} = \sum_{\mathbf{k};\sigma\sigma'} \epsilon_{\sigma\sigma'}(\mathbf{k}) \hat{c}_{\mathbf{k},\sigma}^+ \hat{c}_{\mathbf{k},\sigma'} , \quad (22)$$

$$\epsilon_{\sigma\sigma'}(\mathbf{k}) \equiv \sum_{\gamma\gamma'} Q_{\gamma\gamma'}^{\sigma\sigma'} \epsilon_{\gamma\gamma'}^0(\mathbf{k}) + \eta_{\sigma\sigma'} , \quad (23)$$

where the tensor elements $Q_{\gamma\gamma'}^{\sigma\sigma'}$ are known functions of the parameters m_{Γ} and the density matrix $C_{\sigma\sigma'}$, and $\eta_{\sigma\sigma'}$ are Lagrange parameters which act as effective on-site energies, see

Sections 6 and 7. The one-particle eigenvalues ($\equiv E_{\mathbf{k},\tau}$) of \hat{T}^{eff} can be interpreted as quasi-particle energies within a Landau–Gutzwiller Fermi-liquid theory, see [31] and Section 7. As we will see in the case of nickel, these eigenvalues are in very good agreement with the band energies as found in ARPES experiments. For the kinetic energy we find

$$E^{\text{kin}}(\{m_{\Gamma}\}, \{C_{\sigma\sigma'}\}, \{\eta_{\sigma\sigma'}\}) = \sum_{\sigma\sigma', \gamma\gamma'} Q_{\gamma\gamma'}^{\sigma\sigma'}(\{m_{\Gamma}\}, \{C_{\sigma\sigma'}\}) \sum_{\mathbf{k}} \epsilon_{\gamma\gamma'}^0(\mathbf{k}) \langle \Psi_0 | \hat{c}_{\mathbf{k},\sigma}^+ \hat{c}_{\mathbf{k},\sigma'} | \Psi_0 \rangle, \quad (24)$$

The local density matrix $C_{\sigma\sigma'}$, via eq. (21), and, therefore, the variational energy E^{var} may be considered as functions of m_{Γ} and $\eta_{\sigma\sigma'}$. The remaining numerical task is then to minimize E^{var} with respect to these parameters. There are, however, still up to $(2N_o)^2 + 1$ constraints which have to be respected during the minimization, see (47)–(50). For example, the completeness of the states $|\Gamma\rangle_{\mathbf{m}}$ apparently leads to the constraint $\sum_{\Gamma} m_{\Gamma} = 1$. There is no simple recipe for the most efficient way to implement these constraints in the numerical minimization procedure. In previous works [29, 30] we have proposed the following strategy: We perform a transformation of the local orbital basis onto a new one in which the local density matrix is diagonal. In this new basis, the main $(2N_o)^2$ constraints could then be implemented by the diagonalization of a $2N_o$ -dimensional matrix which we called the ‘ Z -matrix’. In the following section we present results using this strategy. The final numerical results should not be affected by the way the constraints are implemented.

3 Results for ferromagnetic nickel

In this section we first specify our model parameters. Then we give some details of our variational calculations. Finally, we discuss our results for the quasi-particle band structure and the magnetic anisotropy.

3.1 Model specifications

The multi-band Gutzwiller theory is not an ab-initio theory. It is based on a multi-band Hubbard Hamiltonian whose parameters need to be specified. For metallic systems, the use of a Hubbard model is well justified: screening is very efficient so that the effects of the Coulomb interaction between electrons at distances larger than the inverse Fermi wave number k_F^{-1} can be incorporated in the ‘bare’ band structure, and only the local, effective Coulomb matrix elements need to be taken into account explicitly.

3.1.1 Electron-transfer amplitudes and local potential terms

For nickel, we consider a minimal model which includes only those bands which are partly filled within a paramagnetic LDA calculation. Therefore, our multi-band Hubbard Hamiltonian \hat{H} comprises of 18 spin orbitals, namely $3d$, $4s$, and $4p$. The non-magnetic local-density approximation to DFT provides the LDA band structure $\epsilon_{\tau}^{\text{LDA}}(\mathbf{k})$. We represent the bare energy-band matrix elements $\epsilon_{\sigma\sigma'}^0(\mathbf{k})$ in the kinetic energy operator \hat{T} in terms of real electron-transfer integrals $t^{\sigma\sigma'}(\mathbf{r})$ in the two-center approximation [32] which range up

to third nearest neighbors, $N_{\mathbf{r}} \leq 3$. We choose these parameters and the local potential terms $\epsilon_{\sigma\sigma'}$ in such a way that our tight-binding fit reproduces the LDA band structure. In this fit we include information on the symmetry of the single-particle states [33].

$N_{\mathbf{r}}$	$ss\sigma$	$sp\sigma$	$sd\sigma$	$pp\sigma$	$pp\pi$
1	-1.0292	1.2047	-0.5933	1.2144	-0.5284
2	-0.1039	0.2234	-0.1089	0.5989	-0.2205
3	-0.0050	-0.0223	-0.0223	0.0137	0.0076
	$pd\sigma$	$pd\pi$	$dd\sigma$	$dd\pi$	$dd\delta$
1	-0.6960	0.2300	-0.4780	0.3150	-0.0481
2	-0.2092	0.0524	-0.0848	0.0336	-0.0007
3	-0.0439	-0.0023	-0.0245	-0.0011	0.0024

Table 1: Electron-transfer parameters $t_{\sigma\sigma'}(\mathbf{r})$ to $N_{\mathbf{r}}$ -th neighbors (all energies in eV).

For the optimal choice, the \mathbf{k} -averaged root-mean-square deviation between our tight-binding fit and the LDA band structure up to 2 eV above the Fermi energy is 15 meV for the $3d$ bands and for the $4sp$ bands. Our values of the electron-transfer parameters are summarized in Table 1. These model parameters have already been used for the calculations reported in Refs. [30, 34].

For the on-site parameters we find for both spin species

$$\begin{aligned}
\epsilon_{4s,4s} &\equiv \epsilon_s = 5.6022 \text{ eV} , \\
\epsilon_{4p,4p}^{\text{LDA}} &\equiv \epsilon_p^{\text{LDA}} = 8.5335 \text{ eV} , \\
\epsilon_{4p,4p} &\equiv \epsilon_p^{\text{shift}} = 7.7835 \text{ eV} , \\
\epsilon_{3d(t_{2g}),3d(t_{2g})} &\equiv \epsilon_{t_{2g}} = -0.0290 \text{ eV} , \\
\epsilon_{3d(e_g),3d(e_g)} &\equiv \epsilon_{e_g} = 0.0436 \text{ eV} .
\end{aligned} \tag{25}$$

where ϵ_p^{LDA} is the result from the fit to LDA and $\epsilon_p^{\text{shift}}$ is used in practical calculations for a better agreement between our Gutzwiller theory and ARPES experiments for nickel, see below. For the total crystal-field splitting we find $\epsilon_{\text{cf}} = \epsilon_{t_{2g}} - \epsilon_{e_g} = -0.0726 \text{ eV}$.

The energetically highest-lying state of pure d character is X_5 (purely t_{2g}), 0.18 eV above the Fermi energy. The state X_2 (purely e_g) lies 0.025 eV above E_{F} . The width of the $3d$ bands can be estimated from $E(X_5) - E(X_1) = 4.45 \text{ eV}$ (X_1 is predominantly of $d(e_g)$ character), or from $E(X_5) - E(L_1) = 4.63 \text{ eV}$ (L_1 is predominantly $d(t_{2g})$).

Next, we address the $L_{2'}$ -state. Experiment locates this state at about 1.0 eV below E_{F} . The SDFT calculations for ferromagnetic nickel as well as our Gutzwiller theory find the $L_{2'}$ -state about 0.3 eV below the Fermi energy when we use the LDA $4p$ orbital energy $\epsilon_p^{\text{LDA}} = 8.5335 \text{ eV}$. Therefore, we shift the $4p$ orbital energy by 0.75 eV to $\epsilon_p^{\text{shift}} = 7.7835 \text{ eV}$, and find the $L_{2'}$ -state 0.97 eV below E_{F} . In the following we present results which use $\epsilon_p^{\text{shift}} = 7.7835 \text{ eV}$. This choice enhances the $4p$ partial density by approximately 0.1 electron and, correspondingly, enhances the $3d$ hole charge by the same amount so that we work with $n_d = 8.78$ [24]. The remaining 1.22 valence electrons are about evenly split between the $4s$ level and the three $4p$ levels.

3.1.2 Atomic interactions

As described above, the paramagnetic LDA calculation provides a first single-particle contribution to the local Hamiltonian,

$$\hat{H}_{\text{at}}^{(1a)} = \sum_{\mathbf{m}, \sigma} \epsilon_{\sigma\sigma} \hat{c}_{\mathbf{m}, \sigma}^+ \hat{c}_{\mathbf{m}, \sigma} \quad (26)$$

with $|\sigma\rangle = |4s, 4p, 3d\rangle \otimes |\uparrow, \downarrow\rangle$. In addition to these single-particle contributions, we include the spin-orbit interaction for the $3d$ electrons only, $|\sigma\rangle = |3d\rangle \otimes |\uparrow, \downarrow\rangle$. Hereby we restrict ourselves to the dominant, purely atomic contributions of the form

$$\hat{H}_{\text{at}}^{(1b)} = \sum_{\mathbf{m}, \sigma, \sigma'} \frac{\zeta}{2} \langle \sigma | \hat{l}_x \tilde{\sigma}_x + \hat{l}_y \tilde{\sigma}_y + \hat{l}_z \tilde{\sigma}_z | \sigma' \rangle \hat{c}_{\mathbf{m}, \sigma}^+ \hat{c}_{\mathbf{m}, \sigma'} \quad (27)$$

Here, ζ is the strength of the spin-orbit coupling, $\tilde{\sigma}_{x,y,z}$ are the three Pauli matrices, and $\hat{l}_{x,y,z}$ are the Cartesian components of the vector operator for the angular momentum. For the spin-orbit coupling constant we choose $\zeta = 0.080$ eV as in Refs. [35, 36].

The second part of the local interaction is the two-particle Coulomb interaction,

$$\hat{H}_{\text{at}}^{(2)} = \sum_{\mathbf{m}} \sum_{\sigma_1, \sigma_2, \sigma_3, \sigma_4} \mathcal{U}(\sigma_1, \sigma_2; \sigma_3, \sigma_4) \hat{c}_{\mathbf{m}, \sigma_1}^+ \hat{c}_{\mathbf{m}, \sigma_2}^+ \hat{c}_{\mathbf{m}, \sigma_3} \hat{c}_{\mathbf{m}, \sigma_4} \quad (28)$$

The intra-atomic interactions in the $4s$ and $4p$ shell are rather weak when compared to the broad $4sp$ energy bands. Thus, we expect only small correlation effects in these bands. We also neglect correlations between $4sp$ electrons and $3d$ electrons beyond those contained in the LDA band structure. This is a more serious approximation as we neglect magnetic polarization effects on the $4sp$ bands and thus may underestimate the $4sp$ contribution to the magnetic moment. Under these assumptions, the spin-orbit sum in (28) runs over the $3d$ orbitals only. The Hamiltonian of the full atomic problem, $\hat{H}_{\text{at}} = \hat{H}_{\text{at}}^{(1a)} + \hat{H}_{\text{at}}^{(1b)} + \hat{H}_{\text{at}}^{(2)}$, provides the matrix elements between two atomic configurations I_1 and I_2 in (15),

$$U_{I_1, I_2} = \mathbf{m} \langle I_1 | \hat{H}_{\text{at}}^{(1a)} + \hat{H}_{\text{at}}^{(1b)} + \hat{H}_{\text{at}}^{(2)} | I_2 \rangle_{\mathbf{m}} \quad (29)$$

The atomic eigenstates $|\Gamma\rangle_{\mathbf{m}}$ can be written as product states,

$$|\Gamma\rangle_{\mathbf{m}} = |\Gamma_{3d}\rangle_{\mathbf{m}} |\Gamma_{4s}\rangle_{\mathbf{m}} |\Gamma_{4p}\rangle_{\mathbf{m}} \quad (30)$$

In our Gutzwiller theory we correlate the $3d$ states $|\Gamma_{3d}\rangle_{\mathbf{m}}$ only, i.e., the variational parameter λ_{Γ} is independent of the $4sp$ configuration $|\Gamma_{4s}\rangle_{\mathbf{m}} |\Gamma_{4p}\rangle_{\mathbf{m}}$. This leads to a numerically tractable problem with $\mathcal{O}(10^3)$ variational parameters for the atomic $3d$ states.

Naturally, we must not completely ignore the Coulomb interaction of the $4sp$ electrons. In this case a big charge flow from the $3d$ to the $4sp$ bands and unphysically small occupations of the $3d$ shell would result. One way to overcome the charge flow problem is to introduce a chemical potential which keeps the $3d$ partial charge fixed during the calculations, $n_d = 8.78$; see [34] for an alternate method which gives essentially the same results.

Gutzwiller theory produces an optimum magnetic (spin-only) moment which is too large by about 10%. It should be mentioned that the SDFM results show a similarly large overshooting of the magnetic moment. To best compare with experiment, we thus carry out calculations at fixed magnetic moment for the total energy, with either the spin-only moment fixed to the (spin-only) experimental value of $\mu_{\text{spin}} = 0.55\mu_{\text{B}}$ [30] or with the total magnetic moment fixed to the full experimental moment of $\mu = 0.606\mu_{\text{B}}$ when the spin-orbit coupling is included [37].

3.1.3 Parameters for the Coulomb interaction

It remains to determine the Coulomb interaction parameters $\mathcal{U}(\sigma_1, \sigma_2; \sigma_3, \sigma_4)$ in (28). In the spherical-atom approximation, there are only three independent interaction parameters, namely the Slater–Condon integrals F_0 , F_2 , and F_4 , from which all Coulomb interaction parameters can be determined. We prefer the Racah definition, see [38], where the parameters A , B , and C are used which are linear combinations of the Slater–Condon integrals.

The spherical-atom approximation is excellent in cubic systems. In principle, the Coulomb interaction among $3d(t_{2g})$ electrons may differ from the Coulomb interaction among $3d(e_g)$ electrons because the radial parts of their orbital wave functions can be different. Measurements of d - d transitions of magnetic impurities with cubic site symmetry in non-magnetic oxide hosts show that these differences are marginal. The d^3 multiplets 3H and 3P , which are accidentally degenerate in spherical-atom approximation, split by cubic two-particle corrections but not by the crystal field. However, they are found to be degenerate within the experimental resolution of some meV [38]. In test calculations we have used different A parameters for $d(t_{2g})$ electrons and $d(e_g)$ electrons but we have not found any features in our quasi-particle energies which would indicate a failure of the spherical-atom approximation.

The Racah parameters B and C are related to the Slater integrals F_2 and F_4 . They determine the splitting of the multiplets of a specific $3d^n$ configuration. They can be determined experimentally from d - d transition spectra for magnetic impurity ions in non-magnetic insulating hosts. Typical values for all kinds of transition metal ions are tabulated in [38]. It is found experimentally that the ratio C/B varies smoothly between 4 and 5; $C/B = 4$ is obtained theoretically when hydrogen $3d$ wave functions are used. Experimentally, the values for B and C for Ni^{2+} and Ni^{3+} ions are known [38]. When we linearly extrapolate these values to a neutral atom we find our values for nickel as $B = 0.09 \text{ eV}$ and $C = 0.40 \text{ eV}$ so that we employ a ratio $C/B = 4.4$. The values for B and C are close to the ‘bare’ atomic values, i.e., the screening appears to be of little importance to B and C . For a fixed ratio C/B , we may replace the two interaction parameters B and C by a single effective parameter J , as is quite often done in the LDA+ U literature. This exchange coupling J is related to B and C by

$$\frac{B}{2} + \frac{C}{5} = \frac{J}{7}. \quad (31)$$

For our nickel values for B and C we find $J = 0.88 \text{ eV}$, a value very similar to the ones used by Anisimov et al. [12] and others.

The Racah parameter A (basically the U parameter of the Hubbard model) determines the separation of the various d^n multiplets. The ‘bare’ values, as calculated, e.g., from atomic wave-functions are of the order of 25 eV, as discussed already in Herring’s book on magnetism [39] and confirmed recently in [40]. There is a technique to extract U parameters using ‘constraint’ density-functional theory and supercell geometries. It has been found that for minimum-basis models the U -values are smallest. For example, in the case of the cuprates, values $U \leq 2$ eV were found for a single-band Hubbard model whereas a three-band model including the oxygen $2p$ states employs $U_{dd} \approx 8$ eV [41]. Similar results have been found in the case of BaBiO₃ [42]. For $3d$ band models, values of $U = 4 \dots 6$ eV have been reported [43]. For the $4s$ - $4p$ - $3d$ multi-band case of nickel, no such calculations are available but values $U \approx 10$ eV appear to be reasonable. We choose A in such a way that our Gutzwiller theory reproduces the experimental $3d$ band width. For our 18 orbital basis we find $A = 9$ eV to reproduce best the quasi-particle $3d$ band width $W = 3.3$ eV; a value of $A = 12$ eV leads to $W = 3.0$ eV. If we worked with a model of only ten $3d$ spin orbitals, the corresponding band-width reduction is achieved for $A \approx 4$ eV.

3.2 Details of the calculations

The minimization problem consists of two parts. We have to optimize the Hubbard interaction through the variational parameters m_Γ (‘internal’ variation) and the kinetic energy through the one-particle product state $|\Psi_0\rangle$ and its quasi-particle excitation spectrum (‘external’ variation). During the variations we keep the partial densities fixed through a ‘chemical potential’ and work for fixed magnetization (spin-only in the absence of spin-orbit coupling). These two minimization steps are done recursively. The separation of ‘internal’ and ‘external’ minimization offers the advantage that computer time-consuming integrations in momentum space are reduced to a minimum.

Experimentally, the anisotropy energy is $E_{\text{aniso}} \approx -3 \mu\text{eV}$ per atom. Therefore, our total-energy calculations must reach an accuracy of $\mathcal{O}(0.1 \mu\text{eV})$ per atom.

3.2.1 Band calculations

The calculation of the kinetic energy contribution to the variational ground-state energy requires the sum over quasi-particle energies up to the Fermi energy E_F . In the absence of the spin-orbit coupling we use the point-group symmetry of the fcc lattice and calculate all quantities in the irreducible part of the Brillouin zone. This amounts to a reduction of the zone volume by a factor of 48. In order to generate our mesh in momentum space, we divide the distance between the Γ and the X point by 20. This is the standard \mathbf{k} -mesh used in all our calculations. For the calculations with cubic symmetry this results in 916 points and $4.0 \cdot 10^3$ tetrahedra for the mapping of the Fermi surface in the irreducible part of the Brillouin zone. For the calculations including spin-orbit coupling, we use the same mesh. Now that the \mathbf{k} -summation runs over the full Brillouin zone, we sample over $3.4 \cdot 10^4$ \mathbf{k} -points and $1.6 \cdot 10^5$ tetrahedra.

For the numerical integrations required for the calculation of the kinetic energy, we use the tetrahedron method as described in [44]. Additionally, in all calculations we

employ a refinement of the numerical integration near E_F whereby we check whether or not a tetrahedron contains states within a certain energy shell around E_F . If so, we divide the tetrahedron into eight smaller ones and repeat the integration using the smaller tetrahedra. For the spin-only (full moment) nickel calculations our integration refinement near E_F results in $4.0 \cdot 10^4$ ($1.7 \cdot 10^6$) additional tetrahedra in momentum space close to E_F .

In order to achieve an accuracy of 10^{-7} eV for the ground-state energy, we need to suppress numerical noise. For example, a numerical integration yields the elements of the single-particle on-site density matrix \tilde{C} (21). For cubic symmetry, some diagonal elements should be identical but they show some scattering. Even worse, off-diagonal elements which should be zero by symmetry are finite, of the order $\mathcal{O}(10^{-6})$, albeit we perform our calculations in double precision. The main reason for the numerical noise is the limited accuracy of the tetrahedral method and of the integration refinement. In principle, numerical noise can be reduced by choosing a finer \mathbf{k} -mesh; finite computational resources bar this route to higher accuracy. Instead, we take advantage of all symmetries of the problem, e.g., in a system with cubic symmetry the on-site density matrix \tilde{C} becomes diagonal. Therefore, off-diagonal matrix elements can be set to zero, and diagonal elements are replaced by their average.

3.2.2 Variational procedure

The variational energy has to be minimized with respect to the internal variational parameters m_Γ and the external parameters $\eta_{\sigma\sigma'}$. The latter can be interpreted as the effective on-site energies, crystal-field splittings, exchange splittings, and spin-orbit couplings. As shown in Section 3.1 for cubic nickel, symmetry allows three external variational parameters for the $3d$ electrons: the effective crystal-field splitting $\epsilon_{\text{cf}}^{\text{eff}}$ and the effective exchange splittings $\Delta^{\text{eff}}(t_{2g})$ and $\Delta^{\text{eff}}(e_g)$, which are different for $3d(t_{2g})$ and $3d(e_g)$ electrons. Symmetry also allows exchange splittings for the $4sp$ orbitals but these turn out to be of very minor importance, as long as we do not include the atomic electron-electron interaction between $3d$ electrons and $4sp$ electrons, see Section 3.1. When we include the spin-orbit coupling (27) there is another external variational parameter, ζ^{eff} , the magnitude of the spin-orbit coupling for our quasi-particle description.

The optimization of the external parameters for a given tensor \tilde{Q} is analogous to the Hartree–Fock variational theory, i.e., it is a familiar self-consistent band-structure problem. We would reproduce the results of a pure mean-field LDA+U approach if we set $Q_{\gamma\gamma'}^{\sigma\sigma'} = \delta_{\gamma,\sigma}\delta_{\gamma',\sigma'}$. In the case of nickel, however, we found that \tilde{Q} deviates significantly from this simple diagonal form. This explains why mean-field theories fail to describe the electronic properties of nickel correctly.

The variation of the internal variational parameters m_Γ was the centerpiece of our programming efforts. All our schemes use random number generators for the starting values of the variational parameters so that we can easily test the stability of our results. We repeat the runs for different seeds and study the scatter of the results, not only in the total energy, but also in the values of the individual variational parameters.

For fixed external variational parameters, the kinetic energy (24) changes only due to the internal variational parameters m_Γ . The tensor \tilde{Q} in (24) is a product of matrices \tilde{q}

whose entries can be written in the form

$$q_{\sigma_1, \sigma_2} = \sum_{\Gamma_1, \Gamma_2} \Sigma(\sigma_1, \sigma_2; \Gamma_1, \Gamma_2) \sqrt{m_{\Gamma_1}} \sqrt{m_{\Gamma_2}}. \quad (32)$$

Most of the elements of the tensor $\tilde{\Sigma}$ can be prepared before we start the variation of the internal variational parameters, i.e., they do not change during the optimization of the parameters m_Γ . Note that the eigenvalues and eigenvectors of the matrix \tilde{Z} feed into the tensor $\tilde{\Sigma}$. The matrix \tilde{Z} of size 10×10 has to be recalculated and diagonalized at each internal variation step as it ensures fulfillment of the conditions (47) and (48), see Section 4.1. However, only a few of the elements in $\tilde{\Sigma}$ are affected by these recalculations.

The present code simply varies each m_Γ one by one, calculates the matrix \tilde{Z} and the corrections to the matrix \tilde{q} in each step, computes the matrices \tilde{q} and \tilde{C} , and carries out the total-energy summations both for the interaction energy and the kinetic energy. The use of the matrix \tilde{q} considerably speeds up the calculation and variation of \tilde{Q} and thus of the kinetic energy.

A large number of variational parameters is very small, e.g., the probability m_Γ for a local configuration Ni^{7+} is tiny. We use a cut-off below which such variational parameters are set to zero and are no longer varied. In general, big variational parameters influence the energy more strongly than small ones so that we vary big variational parameters more often. Typically, we perform $1.0 \cdot 10^5$ to $5.0 \cdot 10^5$ variations to reach convergence. Hereby, the energy reduction in the last $2.0 \cdot 10^4$ variations is less than $0.1 \mu\text{eV}$. When we repeat the run for different seeds, the total energy scatters by less than $1 \mu\text{eV}$. The individual scatter of band and interaction energies is of the order $\mathcal{O}(\mu\text{eV})$. The scatter in the most significant m_Γ values is of the order $\mathcal{O}(10^{-4})$, the same holds true for the diagonal elements of the matrix \tilde{q} .

3.3 Quasi-particle band structure without spin-orbit coupling

First we address the case where we set the spin-orbit coupling to zero and work with a fixed spin-only moment of $\mu_{\text{spin}} = 0.55$. Figure 1 and table 2 summarize our results which are in very good agreement with ARPES experiments.

Our calculations show the expected dependence of the $3d$ band width on the magnitude of the Racah parameter A via the hopping reduction tensor \tilde{Q} . As can be seen from table 2, the $3d$ band width agrees very well with experiment for $A = 9 \text{ eV}$. The Racah parameters only indirectly influence the quasi-particle bands through the matrix \tilde{Q} whose elements determine the reduction of the electron-transfer amplitudes. Modifications of the values for A , B , and C cause overall energy shifts but they only weakly influence specific band states. Now that the value of A is so much bigger than B and C , there is very little dependence of the $3d$ band width on the value of the Racah parameters B and C .

A central result of our Gutzwiller theory is the anisotropic exchange splitting. The magnetization of our sample leads to the effective exchange splittings for $3d(e_g)$ states and $3d(t_{2g})$ states, $\Delta^{\text{eff}}(t_{2g}) = 0.25 \text{ eV}$, and $\Delta^{\text{eff}}(e_g) = 0.11 \text{ eV}$ which differ by more than a factor of two. Correspondingly, in the quasi-particle band structure near E_F , states of pure t_{2g} character (e.g., X_5 , $W_{1'}$) exhibit a large splitting of majority and minority spin

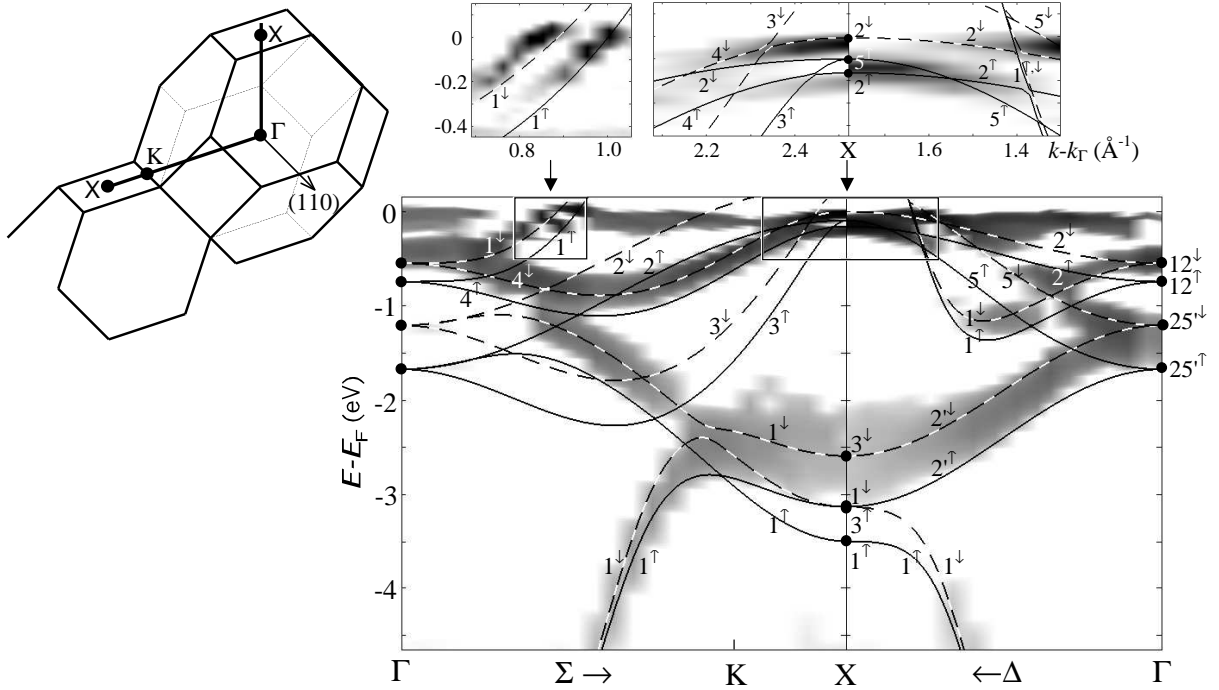


Figure 1: Grey-scale plot of the negative second derivative of the ARPES intensity for nickel with respect to energy, $-d^2I/dE^2$, on a logarithmic scale (insets: linear scale) for the ΓKX and ΓX directions of the Brillouin zone. The dispersionless structure at E_F is due to a residual Fermi edge resulting from indirect transitions. Some bands (Δ_2 , X_1 , Σ_2 , Σ_3 , Σ_1 towards Γ) are not seen due to unfavorable matrix elements, depending on geometry and chosen final state [30]. Theoretical curves are G-DFT, see table 2.

states of about 400 meV whereas the states with pure e_g character (e.g., X_2) exhibit small splittings of about 150 meV to 200 meV, see table 2. An important consequence of this anisotropy is the result that the state $X_{2\downarrow}$ lies slightly below the Fermi energy. This result is robust in all our calculations with Gutzwiller theory, e.g, it also applies for $A = 12$ eV.

The large anisotropy of the exchange splitting has been found experimentally by spin-polarized ARPES studies along the Λ -line of the Brillouin zone [45], and is well reproduced by our Gutzwiller theory, see table 2. In contrast, the SDFT energy bands show a much larger but rather isotropic exchange splitting because the exchange-correlation potential is constructed both from superposed $3d(t_{2g})$ and $3d(e_g)$ charge densities, i.e., the exchange-correlation potential is independent of the orbitals. In our Gutzwiller theory the two values for the exchange splittings result from two independent variational parameters.

It is relatively easy to understand the reason for the large anisotropy of the exchange splittings. The width of the $3d(t_{2g})$ bands is mainly determined by the first-neighbor electron-transfer integral $(dd\sigma)_1$, the largest $3d$ - $3d$ matrix element, see table 1. The width of the $3d(e_g)$ bands does not depend on the $(dd\sigma)_1$ integral, but only on the much smaller $(dd\sigma)_2$ integral to second nearest neighbors. In addition there is some first-neighbor $3d(e_g)$ - $3d(t_{2g})$ hybridization via the large $(dd\pi)_1$ integral. Thus, the most strongly anti-

bonding bands are the $3d(t_{2g})$ bands which form the top of the $3d$ bands. Electron-electron interaction enforces the exchange splitting of the bands up to the point where the limit of strong ferromagnetism is reached and the majority spin bands are completely filled. In the minority spin bands, some energy can be gained when the occupation of the anti-bonding $3d(t_{2g})$ bands is reduced, at the expense of the occupation of the top of the $3d(e_g)$ bands, i.e., of the occupation of the $X_{2\downarrow}$ state.

Symmetry	Character	Experiment	Reference	G-DFT	SDFT
$\langle\Gamma_1\rangle$	S	8.90 ± 0.30	[30]	8.86	8.96[-0.11]
$\langle\Gamma_{25'}\rangle$	T	1.30 ± 0.06	[30]	1.44[0.46]	1.99[0.43]
$\langle\Gamma_{12}\rangle$	E	0.48 ± 0.08	[30]	0.65[0.195]	0.86[0.41]
$\langle X_1\rangle$	sE	3.30 ± 0.20	[22]	3.31[0.36]	4.37[0.20]
$\langle X_3\rangle$	T	2.63 ± 0.10	[30]	2.86[0.54]	3.82[0.37]
$X_{2\uparrow}$	E	0.21 ± 0.03	[30]	0.165	0.35
$X_{2\downarrow}$	E	0.04 ± 0.03	[30]	0.01	-0.09
$X_{5\uparrow}$	T	0.15 ± 0.03	[30]	0.10	0.23
$\Delta_{e_g}(X_2)$	E	0.17 ± 0.05	[30]	0.155	0.44
$\Delta_{t_{2g}}(X_5)$	T	0.33 ± 0.04	[21]	0.38	0.56
$\langle K_1\rangle$	sptE	3.10 ± 0.20	[22]	2.76[0.33]	3.66[0.26]
$\langle K_2\rangle$	spTe	2.48 ± 0.06	[22]	2.59[0.50]	3.37[0.32]
$\langle K_3\rangle$	pT	0.90 ± 0.20	[22]	1.36[0.41]	1.73[0.37]
$\langle K_4\rangle$	pE	0.47 ± 0.03	[30]	0.51[0.185]	0.70[0.41]
$\langle L_1\rangle$	sT	3.66 ± 0.10	[30]	3.51[0.515]	4.56[0.23]
$\langle L_3\rangle$	tE	1.43 ± 0.07	[30]	1.51[0.34]	2.02[0.40]
$L_{3\uparrow}$	Te	0.18 ± 0.03	[30]	0.22	0.38[0.50]
$\langle L_{2'}\rangle$	P	1.00 ± 0.20	[22]	0.97[0.0]	0.24[-0.12]
$\langle W_{2'}\rangle$	pE	2.60 ± 0.20	[22]	2.66[0.31]	3.46[0.24]
$\langle W_3\rangle$	pT	1.70 ± 0.20	[22]	2.04[0.47]	2.69[0.36]
$\langle W_1\rangle$	sE	0.65 ± 0.10	[22]	0.69[0.20]	0.94[0.39]
$W_{1'\uparrow}$	T	0.15 ± 0.10	[22]	0.11	0.23[0.56]
$\langle\Lambda_{3;1/3}\rangle$	ptE	$0.57[0.16\pm 0.02]$	[45]	0.67[0.22]	0.90[0.42]
$\langle\Lambda_{3;1/2}\rangle$	ptE	$0.50[0.21\pm 0.02]$	[45]	0.55[0.26]	0.76[0.44]
$\langle\Lambda_{3;2/3}\rangle$	pTE	$0.35[0.25\pm 0.02]$	[45]	0.33[0.29]	0.49[0.48]

Table 2: Binding energies in eV with respect to the Fermi energy E_F (> 0 for occupied states). $\langle\dots\rangle$ indicates the spin average, error bars in the experiments without spin resolution are given as \pm . Theoretical data show the spin average and the exchange splittings in square brackets. The second column denote the orbital character of the states, $t \equiv t_{2g}$, $e \equiv e_g$, capital letters: dominant character. The spin-polarized data $\langle\Lambda_{3;f}\rangle$ were taken at fractions f of the ΓL distance, with the emphasis on the analysis of the exchange splittings. G-DFT and SDFT calculations are without spin-orbit coupling and a fixed spin-only moment of $\mu_{\text{spin}} = 0.55\mu_B$.

3.4 Magnetic anisotropy

We now turn on the spin-orbit coupling. Again, we perform fixed-moment calculations, now with the full magnetic moment $\mu = 0.606 \mu_B$. Our total-energy calculations including spin-orbit coupling are two to three orders of magnitude more time consuming than the calculations discussed in Section 3.3 because our \mathbf{k} -sums run over the full Brillouin zone, all hundred elements of the matrix \tilde{q} must be calculated and all thousand internal variational parameters must be optimized, and additional external variational parameters appear, e.g., the effective spin-orbit coupling ζ^{eff} .

Symm.	Char.	G-DFT	G-DFT(SO)	Symm.	Char.	G-DFT	G-DFT(SO)
$\Gamma_{25'\uparrow}$	T	1.67	1.74	$\Lambda_{3;1/3\uparrow}$	ptE	0.78	0.81 ; 0.80
			1.67				0.76 ; 0.78
			1.17				
$\Gamma_{25'\downarrow}$	T	1.21	1.25	$\Lambda_{3;1/3\downarrow}$	ptE	0.57	0.61 ; 0.59
			1.21				0.56 ; 0.57
			1.17				
$X_{2\uparrow}$	E	0.17	0.19	$\Lambda_{3;1/2\downarrow}$	ptE	0.42	0.72 ; 0.70
$X_{2\downarrow}$	E	0.01	0.02				0.66 ; 0.69
$X_{5\uparrow}$	T	0.10	0.13	$\Lambda_{3;2/3\uparrow}$	pTE	0.47	0.47 ; 0.44
			0.11				0.39 ; 0.41
$X_{5\downarrow}$	T	-0.28	-0.27	$\Lambda_{3;2/3\downarrow}$	pTE	0.19	0.52 ; 0.50
			-0.32				0.45 ; 0.48
$L_{3\uparrow}$	Te	0.22	0.26 ; 0.24				0.22 ; 0.20
			0.20 ; 0.22			0.16 ; 0.18	

Table 3: Theoretical binding energies in eV with respect to the Fermi energy E_F (> 0 for occupied states) with and without spin-orbit coupling. The second column denote the orbital character of the states, $t \equiv t_{2g}$, $e \equiv e_g$, capital letters: dominant character. For the calculations without spin-orbit coupling, G-DFT, we used a spin-only moment of $\mu_{\text{spin}} = 0.55 \mu_B$. In the spin-orbit calculation, G-DFT(SO), we worked with a fixed moment of $0.606 \mu_B$ along the (111)-direction. The directions Λ and the L -points in the Brillouin zone are not equivalent: the first and the second energy belong to the directions parallel and perpendicular to (111), respectively.

Our optimal ground state displays an orbital moment of $\mu_{\text{orb}} = 0.052 \mu_B$ which agrees very well with the experimental value of $\mu_{\text{orb}} = 0.0507 \mu_B$ [1]. In the Hartree-Fock limit of our method, $\lambda_\Gamma \equiv 1$, we obtain $\mu_{\text{orb,HF}} = 0.032 \mu_B$. Obviously, the orbital-moment contribution to the total moment almost doubles when we apply our Gutzwiller theory. This is due to the fact that correlations induce non-diagonal elements in the matrix \tilde{q} ; they

become nonzero because the spin-orbit coupling lifts the cubic symmetry. An analysis of the quasi-particle bands shows that the non-diagonal elements of the matrix \tilde{q} induce electron transfers with spin flips in the effective single-particle Hamiltonian. These processes give an additional contribution to the orbital moment. The effective value for the spin-orbit coupling becomes smaller, $\zeta^{\text{eff}} = 0.070$ eV for the optimum ground-state energy. This is a 12% reduction compared to the bare spin-orbit coupling constant $\zeta = 0.080$ eV. Calculations with a fixed $\zeta^{\text{eff}} = \zeta$ yield higher ground-state energies and an approximately 10% larger orbital moment.

The central external variational parameters, the effective exchange splittings $\Delta^{\text{eff}}(t_{2g})$ and $\Delta^{\text{eff}}(e_g)$ as well as the effective crystal-field $\epsilon_{\text{cf}}^{\text{eff}}$, are very similar to the spin-only calculations. Consequently, the quasi-particle bands do not change very much from the quasi-particle bands as described in Section 3.3. However, degeneracies at high-symmetry points and lines are lifted. In table 3, we give some of the energies at high-symmetry points and lines, taken from a calculation where the magnetic moment lies parallel to the (111)-direction, the easy axis of nickel. Near the Fermi energy the splittings should be detectable by high resolution ARPES. Note that the state which derives from the $X_{2\downarrow}$ -state still lies slightly below the Fermi energy.

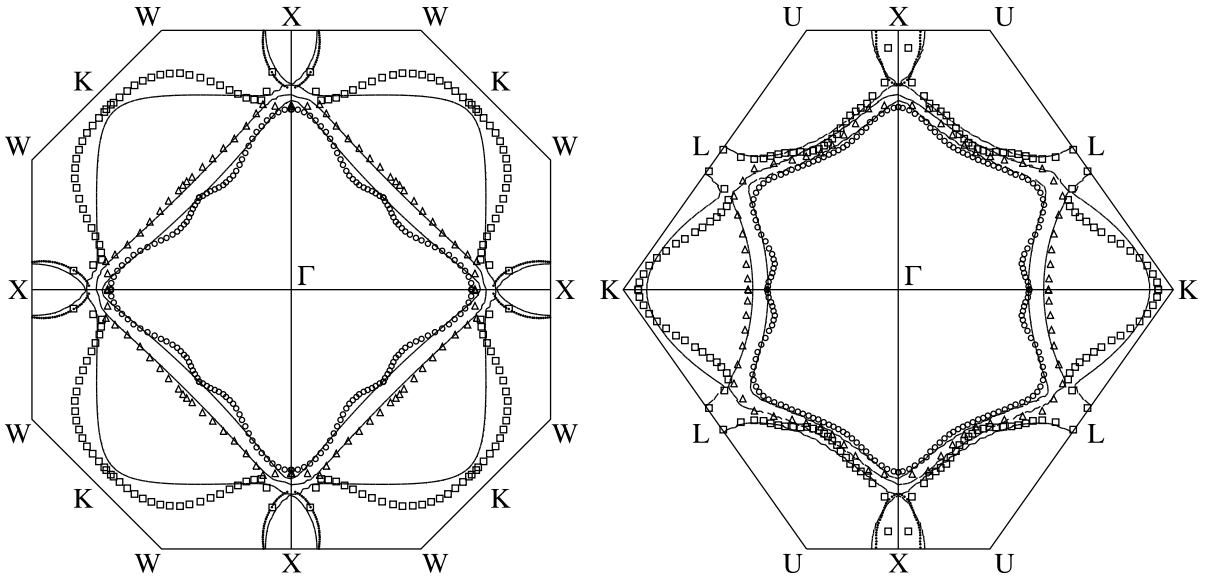


Figure 2: Cut of the Fermi surface with the plane $\Gamma X K$ and the plane $\Gamma X L$ in the Brillouin zone. Open symbols are data of Stark, communicated in [46], filled dots are de-Haas–van-Alphen data from [19], and lines are the results from Gutzwiller theory.

The spin-orbit coupling causes the former majority and minority spin bands to couple so that band crossings of spin-up bands and spin-down bands are avoided. As a consequence, the topology of the Fermi surface changes slightly. These changes affect only a few areas on the Fermi surface. In figure 2, we show a cut of the Fermi surface in the $\Gamma X K$ plane and in the $\Gamma X L$ plane, respectively.

The theoretical Fermi surface agrees very well with the de-Haas–van-Alphen data

of Stark, which have been communicated through the paper of Callaway and Wang [46]. However, the experimental data exhibit oscillations in these cuts which are not reproduced by our Gutzwiller theory. In fact, no band calculation whatsoever has produced these wiggles. We suspect that these wiggles are artifacts of the reconstruction procedure from the raw data: in a magnetic field of several Tesla, the Fermi surface topology itself can change, as we now discuss.

When we align the magnetic moment along the (001)-direction, the quasi-particle energy of the X -states at (100) and at (010) differ from the energy of the (001) X -state; the three states are degenerate when the moment is along the (111) direction. The spin-orbit coupling induces a splitting of the formerly degenerate $X_{2\downarrow}$ state by 30 meV, and the energy of the (001) $X_{2\downarrow}$ -state in the presence of the spin-orbit coupling lies approximately 6 meV above the Fermi energy whereas the other two states lie 25 meV below E_F . Thereby our Gutzwiller theory confirms the scenario put forward by Gersdorf [27].

The differences in ground-energies of the states with the magnetic moment aligned in the (111) direction and with the magnetic moment aligned in the (001) direction, $E_{\text{aniso}} \equiv E_{111} - E_{001}$, is $E_{\text{aniso, Gutz}} \approx -10 \mu\text{eV}$ per atom. Thus we get the correct sign and order of magnitude of the experimental energy difference, $E_{\text{aniso}} = -3 \mu\text{eV}$ per atom. In order to improve the confidence in our results, we have repeated our numerical integrations over the Brillouin zone with a denser mesh but for fixed external variational parameters. Our calculations using a denser mesh with up to $2.5 \cdot 10^5$ \mathbf{k} -points in the Brillouin zone confirm the result of a (111) easy axis in nickel. Therefore, we are confident that Gutzwiller theory calculations produce reliable results for the magnetic anisotropy energies. Further studies with even larger \mathbf{k} -meshes are in progress.

4 Diagrammatic approach

In this section we develop a general scheme to evaluate expectation values for single-site and two-site operators using the variational analog of Feynman diagrams.

4.1 Conditions

We need to evaluate expectation values of operators \hat{O}_i and $\hat{O}_{i,j} = \hat{c}_{i,\sigma}^{(+)} \hat{c}_{j,\sigma}^{(+)}$ for $i \neq j$ with the wave function (1),

$$\langle \hat{O}_i \rangle_G = \frac{\langle \Psi_0 | \left[\prod_{\mathbf{m} \neq i} \hat{P}_{G|\mathbf{m}}^2 \right] \hat{P}_{G|i} \hat{O}_i \hat{P}_{G|i} | \Psi_0 \rangle}{\langle \Psi_0 | \prod_{\mathbf{m}} \hat{P}_{G|\mathbf{m}}^2 | \Psi_0 \rangle}, \quad (33)$$

$$\langle \hat{O}_{i,j} \rangle_G = \frac{\langle \Psi_0 | \left[\prod_{\mathbf{m} \neq i,j} \hat{P}_{G|\mathbf{m}}^2 \right] \hat{P}_{G|i} \hat{P}_{G|j} \hat{O}_{i,j} \hat{P}_{G|i} \hat{P}_{G|j} | \Psi_0 \rangle}{\langle \Psi_0 | \prod_{\mathbf{m}} \hat{P}_{G|\mathbf{m}}^2 | \Psi_0 \rangle}. \quad (34)$$

The square of the local Gutzwiller correlator can be reduced to

$$\hat{P}_{G|\mathbf{m}}^2 = \sum_{I_1, I_2} \bar{\lambda}_{I_1, I_2|\mathbf{m}} |I_1\rangle_{\mathbf{m}\mathbf{m}} \langle I_2| \quad (35)$$

with

$$\bar{\lambda}_{I_1, I_2 | \mathbf{m}} = \sum_{I'} \lambda_{I_1, I' | \mathbf{m}} \lambda_{I', I_2 | \mathbf{m}} . \quad (36)$$

We aim at a diagrammatic calculation of $\langle \hat{O}_{\mathbf{i}} \rangle_{\mathbf{G}}$ and $\langle \hat{O}_{\mathbf{i}, \mathbf{j}} \rangle_{\mathbf{G}}$. In such an approach, the sites $\mathbf{m} \neq \mathbf{i}, \mathbf{j}$ in (33) and (34) will play the role of inner vertices.

In a first step, we eliminate all local contributions at the inner vertices which arise after the application of Wick's theorem to the numerators in (33) and (34). As in a previous work [29], we expand $\hat{P}_{\mathbf{G} | \mathbf{m}}^2$ in terms of new local operators,

$$\begin{aligned} \hat{P}_{\mathbf{G} | \mathbf{m}}^2 &= 1 + [\hat{P}_{\mathbf{G} | \mathbf{m}}^2]^{\text{HF}} , \\ [\hat{P}_{\mathbf{G} | \mathbf{m}}^2]^{\text{HF}} &= \sum_{I_1, I_2; |I_1| + |I_2| \geq 2} x_{I_1, I_2 | \mathbf{m}} \left(\hat{n}_{I_1, I_2, \mathbf{m}} - [\hat{n}_{I_1, I_2, \mathbf{m}}]^{\text{HF}} \right) , \end{aligned} \quad (37)$$

where

$$\hat{n}_{I_1, I_2, \mathbf{m}} \equiv \prod_{\sigma_1 \in I_1} \hat{c}_{\mathbf{m}, \sigma_1}^+ \prod_{\sigma_2 \in I_2} \hat{c}_{\mathbf{m}, \sigma_2} . \quad (38)$$

The Hartree–Fock operator for an even number $n \geq 4$ of Fermion operators is defined recursively,

$$\begin{aligned} [\hat{a}_1 \dots \hat{a}_n]^{\text{HF}} &\equiv \langle \hat{a}_1 \dots \hat{a}_n \rangle_0 \\ &+ \sum'_{\{\gamma_1, \dots, \gamma_n\}=0} (-1)^{f_s(\{\gamma_i\})} \left\{ \left(\prod_{\ell=1}^n \hat{a}_{\ell}^{\gamma_{\ell}} \right) - \left[\prod_{\ell=1}^n \hat{a}_{\ell}^{\gamma_{\ell}} \right]^{\text{HF}} \right\} \left\langle \prod_{\ell=1}^n \hat{a}_{\ell}^{1-\gamma_{\ell}} \right\rangle_0 \end{aligned} \quad (39)$$

with

$$f_s(\{\gamma_i\}) \equiv \sum_{\ell=1}^n \left(\ell - \frac{1}{2} \right) \gamma_{\ell} . \quad (40)$$

The prime in (39) indicates that $2 \leq \sum_{\ell=1}^n \gamma_{\ell} \leq n - 2$ is even. For $n = 2$ we have

$$[\hat{a}_1 \hat{a}_2]^{\text{HF}} = \langle \hat{a}_1 \hat{a}_2 \rangle_0 . \quad (41)$$

By construction, the operator in (37) generates diagrams with exactly $|I_1|$ ($|I_2|$) non-local lines that enter (leave) the lattice site \mathbf{m} . All diagrams with trivial local Hartree–Fock bubbles are automatically excluded.

For our diagrammatic evaluation we demand that at least four lines meet at every inner vertex,

$$x_{I_1, I_2 | \mathbf{m}} = 0 \quad \text{for} \quad |I_1| + |I_2| = 2 . \quad (42)$$

We can fulfill these conditions by restricting our parameters $\lambda_{I_1, I_2 | \mathbf{m}}$. Using the form (37) together with (42) one easily sees that

$$\langle \hat{P}_{\mathbf{G} | \mathbf{m}}^2 \rangle_0 = 1 , \quad (43)$$

$$\langle \hat{c}_{\mathbf{m}, \sigma}^+ \hat{P}_{\mathbf{G} | \mathbf{m}}^2 \hat{c}_{\mathbf{m}, \sigma'} \rangle_0 = \langle \hat{c}_{\mathbf{m}, \sigma}^+ \hat{c}_{\mathbf{m}, \sigma'} \rangle_0 , \quad (44)$$

$$\langle \hat{c}_{\mathbf{m}, \sigma}^+ \hat{P}_{\mathbf{G} | \mathbf{m}}^2 \hat{c}_{\mathbf{m}, \sigma'}^+ \rangle_0 = \langle \hat{c}_{\mathbf{m}, \sigma}^+ \hat{c}_{\mathbf{m}, \sigma'}^+ \rangle_0 , \quad (45)$$

$$\langle \hat{c}_{\mathbf{m}, \sigma} \hat{P}_{\mathbf{G} | \mathbf{m}}^2 \hat{c}_{\mathbf{m}, \sigma'} \rangle_0 = \langle \hat{c}_{\mathbf{m}, \sigma} \hat{c}_{\mathbf{m}, \sigma'} \rangle_0 \quad (46)$$

must be fulfilled. This follows from the fact that, apart from the trivial term in (37), at least four lines meet at every vertex; a contraction with two ‘external’ fermionic operators leaves at least one uncontracted pair whose local contraction, however, vanishes by construction of new local operators (37). Explicitly,

$$\sum_{I_1, I_2} \bar{\lambda}_{I_1, I_2 | \mathbf{m}} m_{I_1, I_2 | \mathbf{m}}^0 = 1, \quad (47)$$

$$\sum_{I_1 (\sigma \in I_1)} \sum_{I_2 (\sigma' \in I_2)} \bar{\lambda}_{I_1 \setminus \sigma, I_2 \setminus \sigma' | \mathbf{m}} m_{I_1, I_2 | \mathbf{m}}^0 = \langle \hat{c}_{\mathbf{m}, \sigma}^+ \hat{c}_{\mathbf{m}, \sigma'} \rangle_0, \quad (48)$$

$$\sum_{I_1 (\sigma \in I_1)} \sum_{I_2 (\sigma' \in I_2)} \bar{\lambda}_{I_1 \setminus \sigma, I_2 | \mathbf{m}} m_{I_1, I_2 \setminus \sigma' | \mathbf{m}}^0 = \langle \hat{c}_{\mathbf{m}, \sigma}^+ \hat{c}_{\mathbf{m}, \sigma'}^+ \rangle_0, \quad (49)$$

$$\sum_{I_1 (\sigma \in I_1)} \sum_{I_2 (\sigma' \in I_2)} \bar{\lambda}_{I_1, I_2 \setminus \sigma' | \mathbf{m}} m_{I_1 \setminus \sigma, I_2 | \mathbf{m}}^0 = \langle \hat{c}_{\mathbf{m}, \sigma} \hat{c}_{\mathbf{m}, \sigma'} \rangle_0. \quad (50)$$

Here, we introduced the expectation value

$$\begin{aligned} m_{I_1, I_2 | \mathbf{m}}^0 &= \langle \Psi_0 | I_1 \rangle_{\mathbf{m}} \langle I_2 | \Psi_0 \rangle \\ &= \langle \Psi_0 | \hat{n}_{I_1, I_2 | \mathbf{m}} \hat{n}_{I_1 \cup I_2 | \mathbf{m}}^h | \Psi_0 \rangle, \end{aligned} \quad (51)$$

with

$$\hat{n}_{I | \mathbf{m}}^h \equiv \prod_{\sigma \in I} (1 - \hat{n}_{\mathbf{m}, \sigma}) \quad (52)$$

and

$$\hat{n}_{\mathbf{m}, \sigma} \equiv \hat{c}_{\mathbf{m}, \sigma}^+ \hat{c}_{\mathbf{m}, \sigma}. \quad (53)$$

Equations (47)–(50) can be used to fix some of the variational parameters $\lambda_{I_1, I_2 | \mathbf{m}}$, for example those with $|I_1| + |I_2| \leq 1$.

4.2 Diagrammatics

With the help of (37) we expand the product over the squares of local Gutzwiller correlators in (33) [and in (34)] in the form

$$\prod_{\mathbf{m} \neq \mathbf{i}, \mathbf{j}} \hat{P}_{\mathbf{G}; \mathbf{m}}^2 = 1 + \sum_{\mathbf{m}}' [\hat{P}_{\mathbf{G}; \mathbf{m}}^2]^{\text{HF}} + \frac{1}{2} \sum_{\mathbf{m}_1, \mathbf{m}_2}' [\hat{P}_{\mathbf{G}; \mathbf{m}_1}^2]^{\text{HF}} [\hat{P}_{\mathbf{G}; \mathbf{m}_2}^2]^{\text{HF}} + \dots, \quad (54)$$

where the prime on the sums indicates that all lattice sites are different from each other and from \mathbf{i} [and \mathbf{j}]. When Wick’s theorem is applied to the numerators in (33) and in (34) we can introduce *new contractions* between two Fermi operators $\hat{a}_{\mathbf{m}, \sigma}$ and $\hat{a}_{\mathbf{n}, \sigma}$ ($\hat{a} = \hat{c}$ or $\hat{a} = \hat{c}^+$)

$$K_{\mathbf{m}, \sigma; \mathbf{n}, \sigma'}^0 = \langle \hat{a}_{\mathbf{n}, \sigma} \hat{a}_{\mathbf{m}, \sigma'} \rangle_0 - \delta_{\mathbf{n}, \mathbf{m}} \langle \hat{a}_{\mathbf{n}, \sigma} \hat{a}_{\mathbf{n}, \sigma'} \rangle_0. \quad (55)$$

In most cases, $\mathbf{n} \neq \mathbf{m}$ holds and the new definition of a contraction reduces to the usual one because the extra term proportional to $\delta_{\mathbf{n}, \mathbf{m}}$ vanishes. In those cases where Fermi operators on the same site are contracted the contribution must vanish because

we subtracted all local Hartree contributions in $[\hat{P}_{\mathbf{G};\mathbf{m}}^2]^{\text{HF}}$. The new contraction in (55) fulfills this condition.

The application of Wick's theorem thus gives a result which we would have obtained if we had worked with Grassmann operators instead of Fermion operators in the definition of the expectation values; all Grassmann operators $\hat{a}_{\mathbf{i},\sigma}^g$ anti-commute with each other

$$[\hat{a}_{\mathbf{i},\sigma}^g, \hat{a}_{\mathbf{j},\sigma'}^g]_+ = 0, \quad (56)$$

so that local contractions always vanish,

$$\langle \hat{a}_{\mathbf{i},\sigma}^g \hat{a}_{\mathbf{i},\sigma'}^g \rangle_0 = 0. \quad (57)$$

The use of Grassmann operators instead of Fermi operators also shows that we may now drop the restrictions on the lattice sums because all contributions with two lattice sites put equal vanish due to the anti-commutation relation between the corresponding Grassmann operators. In this way we have generated a diagrammatic theory in which lines between two vertices \mathbf{n} and \mathbf{m} are given by the one-particle density matrices $K_{\mathbf{m},\sigma;\mathbf{n},\sigma'}^0$ defined in (55), and $x_{I_1,I_2|\mathbf{m}}$ gives the strength of a vertex $(I_1, I_2|\mathbf{m})$ with $|I_1|$ in-going lines and $|I_2|$ out-going lines.

Now we are in the position to apply the linked-cluster theorem so that all disconnected diagrams in the numerator in (33) [and in (34)] cancel the corresponding denominator. Then, the calculation of the expectation values (33) and (34) is reduced to the sum over all connected diagrams according to the Feynman rules with lines and vertices as defined above.

5 Exact results for infinite coordination number

By construction, at least four lines meet at every inner vertex. Due to the absence of local Hartree–Fock contributions two inner vertices are always connected by at least three independent paths of lines (there is no diagram with a single inner vertex). For lattices with Z nearest neighbors,

$$K_{\mathbf{m},\sigma|\mathbf{n},\sigma'}^0 \sim \mathcal{O}(Z^{-|\mathbf{n}-\mathbf{m}|/2}); \quad (58)$$

for a simple cubic lattice in d dimensions, $Z = 2d$. Therefore, the contribution of all diagrams with inner vertices vanishes at least proportional to $1/\sqrt{d}$ in the limit of infinite dimensions. Thus, not a single diagram needs to be calculated in infinite dimensions, i.e., we arrive at the result

$$\langle \hat{O}_{\mathbf{i}} \rangle_{\mathbf{G}} = \langle \Psi_0 | \hat{P}_{\mathbf{G}|\mathbf{i}} \hat{O}_{\mathbf{i}} \hat{P}_{\mathbf{G}|\mathbf{i}} | \Psi_0 \rangle, \quad (59)$$

$$\langle \hat{O}_{\mathbf{i},\mathbf{j}} \rangle_{\mathbf{G}} = \langle \Psi_0 | \hat{P}_{\mathbf{G}|\mathbf{i}} \hat{P}_{\mathbf{G}|\mathbf{j}} \hat{O}_{\mathbf{i},\mathbf{j}} \hat{P}_{\mathbf{G}|\mathbf{i}} \hat{P}_{\mathbf{G}|\mathbf{j}} | \Psi_0 \rangle \quad (60)$$

in $d = \infty$ dimensions. The result (60) can be further simplified because in $d = \infty$ dimensions there can be only a single line connecting the two external vertices \mathbf{i} and \mathbf{j} .

5.1 Local quantities

Now we address the local operators for the particle densities,

$$\hat{n}_{\mathbf{i},\sigma\sigma'} \equiv \hat{c}_{\mathbf{i},\sigma}^+ \hat{c}_{\mathbf{i},\sigma'} , \quad (61)$$

the pairing densities,

$$\hat{s}_{\mathbf{i},\sigma\sigma'} \equiv \hat{c}_{\mathbf{i},\sigma} \hat{c}_{\mathbf{i},\sigma'} , \quad (62)$$

and the local interaction

$$\hat{H}_{\text{at}} \equiv \sum_{\mathbf{m}} \sum_{J_1, J_2} U_{J_1, J_2 | \mathbf{m}} |J_1\rangle_{\mathbf{m}\mathbf{m}} \langle J_2| . \quad (63)$$

In infinite dimensions we have

$$\begin{aligned} n_{\mathbf{i},\sigma\sigma'} &= \langle \hat{n}_{\mathbf{i},\sigma\sigma'} \rangle_{\text{G}} = \langle \hat{P}_{\text{G}|\mathbf{i}} \hat{c}_{\mathbf{i},\sigma}^+ \hat{c}_{\mathbf{i},\sigma'} \hat{P}_{\text{G}|\mathbf{i}} \rangle_0 \\ &= \sum_{I_1, I_4} N_{I_1, I_4 | \mathbf{i}}^{\sigma\sigma'} m_{I_1, I_4 | \mathbf{i}}^0 . \end{aligned} \quad (64)$$

Here we defined the matrix elements for the local densities as

$$\begin{aligned} N_{I_1, I_4 | \mathbf{i}}^{\sigma\sigma'} &\equiv \sum_{I_2, I_3} \lambda_{I_1, I_2 | \mathbf{i}} \lambda_{I_3, I_4 | \mathbf{i}} \langle I_2 | \hat{c}_{\mathbf{i},\sigma}^+ \hat{c}_{\mathbf{i},\sigma'} | I_3 \rangle_{\mathbf{i}} \\ &= \sum_{I(\sigma\sigma' \notin I)} \lambda_{I_1, I \cup \sigma | \mathbf{i}} \lambda_{I \cup \sigma', I_4 | \mathbf{i}} \text{fsgn}(\sigma, I) \text{fsgn}(\sigma', I) \end{aligned} \quad (65)$$

where

$$\text{fsgn}(\sigma, I) \equiv \langle I \cup \sigma | \hat{c}_{\sigma}^+ | I \rangle \quad (66)$$

is ± 1 if it takes an odd/even number of anti-commutations to shift the state σ to its proper place in the ordered sequence I . Correspondingly, we find

$$\begin{aligned} s_{\mathbf{i},\sigma\sigma'} &= \langle \hat{s}_{\mathbf{i},\sigma\sigma'} \rangle_{\text{G}} = \langle \hat{P}_{\text{G}|\mathbf{i}} \hat{c}_{\mathbf{i},\sigma} \hat{c}_{\mathbf{i},\sigma'} \hat{P}_{\text{G}|\mathbf{i}} \rangle_0 \\ &= \sum_{I_1, I_4} S_{I_1, I_4 | \mathbf{i}}^{\sigma\sigma'} m_{I_1, I_4 | \mathbf{i}}^0 . \end{aligned} \quad (67)$$

Here we defined the matrix elements for the local pairing amplitudes as

$$\begin{aligned} S_{I_1, I_4 | \mathbf{i}}^{\sigma\sigma'} &\equiv \sum_{I_2, I_3} \lambda_{I_1, I_2 | \mathbf{i}} \lambda_{I_3, I_4 | \mathbf{i}} \langle I_2 | \hat{c}_{\mathbf{i},\sigma} \hat{c}_{\mathbf{i},\sigma'} | I_3 \rangle_{\mathbf{i}} \\ &= \sum_{I(\sigma\sigma' \notin I)} \lambda_{I_1, I | \mathbf{i}} \lambda_{I \cup (\sigma\sigma'), I_4 | \mathbf{i}} \text{fsgn}(\sigma, I) \text{fsgn}(\sigma', I) \text{fsgn}(\sigma, \sigma') . \end{aligned} \quad (68)$$

Lastly, along the same lines we find

$$\begin{aligned} E^{\text{at}} &= \langle \hat{H}_{\text{at}} \rangle_{\text{G}} \\ &= \sum_{\mathbf{i}} \langle \hat{P}_{\text{G}|\mathbf{i}} \sum_{J_1, J_2} U_{J_1, J_2 | \mathbf{i}} |J_1\rangle_{\mathbf{i}\mathbf{i}} \langle J_2 | \hat{P}_{\text{G}|\mathbf{i}} \rangle_0 \\ &= \sum_{\mathbf{i}} \sum_{I_1, I_4} \bar{U}_{I_1, I_4 | \mathbf{i}} m_{I_1, I_4 | \mathbf{i}}^0 , \end{aligned} \quad (69)$$

where

$$\bar{U}_{I_1, I_4 | \mathbf{i}} \equiv \sum_{I_2, I_3} \lambda_{I_1, I_2 | \mathbf{i}} \lambda_{I_3, I_4 | \mathbf{i}} U_{I_2, I_3 | \mathbf{i}} . \quad (70)$$

5.2 Single-particle density matrices

Now we evaluate the single-particle density matrix

$$P_{\mathbf{i},\sigma;\mathbf{j},\sigma'} \equiv \langle \hat{c}_{\mathbf{i},\sigma}^+ \hat{c}_{\mathbf{j},\sigma'} \rangle_G \quad (71)$$

and the one-particle pairing matrix

$$S_{\mathbf{i},\sigma;\mathbf{j},\sigma'} \equiv \langle \hat{c}_{\mathbf{i},\sigma} \hat{c}_{\mathbf{j},\sigma'} \rangle_G \quad (72)$$

for $\mathbf{i} \neq \mathbf{j}$.

We start with $\hat{O}_{\mathbf{ij}} = \hat{c}_{\mathbf{i},\sigma}^+ \hat{c}_{\mathbf{j},\sigma'}$ in (34) and evaluate

$$\hat{P}_{G|\mathbf{i}} \hat{c}_{\mathbf{i},\sigma}^+ \hat{P}_{G|\mathbf{i}} = \sum_{I_1, I_4} c_{I_1, I_4|\mathbf{i}, \sigma}^* |I_1\rangle_{\mathbf{ii}} \langle I_4| \quad (73)$$

with

$$\begin{aligned} c_{I_1, I_4|\mathbf{i}, \sigma}^* &\equiv \sum_{I_2, I_3} \lambda_{I_1, I_2|\mathbf{i}} \lambda_{I_3, I_4|\mathbf{i}} \langle I_2 | \hat{c}_{\mathbf{i}, \sigma}^+ | I_3 \rangle_{\mathbf{i}} \\ &= \sum_{I(\sigma \notin I)} \text{fsgn}(\sigma, I) \lambda_{I_1, I \cup \sigma|\mathbf{i}} \lambda_{I, I_4|\mathbf{i}}. \end{aligned} \quad (74)$$

In $d = \infty$ dimensions only a single line can join the two external vertices $\mathbf{i} \neq \mathbf{j}$ in (60). In the first case, the contraction at \mathbf{i} is done with a creation operator $\hat{c}_{\mathbf{i}, \gamma}^+$. There are two possibilities, it can either be $\gamma \in I_1$, with

$$|I_1\rangle_{\mathbf{ii}} \langle I_4| = \left(\text{fsgn}(\gamma, I_1 \setminus \gamma) \hat{n}_{I_1 \setminus \gamma, I_4|\mathbf{i}} \hat{n}_{I_1 \cup I_4|\mathbf{i}}^{\text{h}} \right) \hat{c}_{\mathbf{i}, \gamma}^+, \quad (75)$$

or $\gamma \in \overline{I_1 \cup I_4}$, with

$$|I_1\rangle_{\mathbf{ii}} \langle I_4| = - \left(\text{fsgn}(\gamma, I_4) \hat{n}_{I_1, I_4 \cup \gamma|\mathbf{i}} \hat{n}_{I_1 \cup I_4 \cup \gamma|\mathbf{i}}^{\text{h}} \right) \hat{c}_{\mathbf{i}, \gamma}^+. \quad (76)$$

Altogether, the amplitude for such a process is given by

$$q_{\mathbf{i}, \sigma \gamma}^* \equiv \sum_{I(\gamma \notin I)} \sum_{I'} \text{fsgn}(\gamma, I) (m_{I, I'|\mathbf{i}}^{0(\gamma)} c_{I \cup \gamma, I'|\mathbf{i}, \sigma}^* - m_{I', I \cup \gamma|\mathbf{i}}^0 c_{I', I|\mathbf{i}, \sigma}^*). \quad (77)$$

Here, we introduced the expectation value

$$m_{I, I'|\mathbf{i}}^{0(\gamma)} \equiv \langle \hat{n}_{I, I'|\mathbf{i}} \hat{n}_{I \cup I' \cup \gamma|\mathbf{i}}^{\text{h}} \rangle_0. \quad (78)$$

In previous works [29, 30], the factors $q_{\mathbf{i}, \sigma \gamma}^*$ were denoted by $\sqrt{q_{\mathbf{i}, \sigma \gamma}}$. In general, however, $q_{\mathbf{i}, \sigma \gamma}^*$ is not a positive real number.

The second case is only possible if there are superconducting pairing correlations in $|\Psi_0\rangle$. Then, the line between \mathbf{i} and \mathbf{j} can also be an anomalous propagator, i.e., the contraction at \mathbf{i} can be done with an annihilation operator $\hat{c}_{\mathbf{i}, \gamma}$. Again, we obtain two contributions, $\gamma \in I_4$, which gives

$$|I_1\rangle_{\mathbf{ii}} \langle I_4| = \hat{c}_{\mathbf{i}, \gamma} \left(\text{fsgn}(\gamma, I_2 \setminus \gamma) \hat{n}_{I_1, I_4 \setminus \gamma|\mathbf{i}} \hat{n}_{I_1 \cup I_4|\mathbf{i}}^{\text{h}} \right), \quad (79)$$

and $\gamma \in \overline{I_1 \cup I_4}$, which contributes

$$|I_1\rangle_{\text{ii}}\langle I_4| = \hat{c}_{\mathbf{i},\gamma} \left(\text{fsgn}(\gamma, I_1) \hat{n}_{I_1 \cup \gamma, I_4|\mathbf{i}} \hat{n}_{I_1 \cup I_4 \cup \gamma|\mathbf{i}}^{\text{h}} \right). \quad (80)$$

Therefore, the amplitude for the anomalous process can be written as

$$\bar{q}_{\mathbf{i},\sigma\gamma} \equiv \sum_{I(\gamma \notin I)} \sum_{I'} \text{fsgn}(\gamma, I) (m_{I',I|\mathbf{i}}^{0(\gamma)} c_{I',I \cup \gamma|\mathbf{i},\sigma}^* + m_{I \cup \gamma, I'|\mathbf{i}}^0 c_{I',I'|\mathbf{i},\sigma}^*). \quad (81)$$

With these definitions we find for the one-particle density matrix

$$P_{\mathbf{i},\sigma;\mathbf{j}\sigma'} = \sum_{\gamma\gamma'} \left[q_{\mathbf{i},\sigma\gamma}^* q_{\mathbf{j},\sigma'\gamma'} \langle \hat{c}_{\mathbf{i},\gamma}^+ \hat{c}_{\mathbf{j},\gamma'} \rangle_0 + \bar{q}_{\mathbf{i},\sigma\gamma} \bar{q}_{\mathbf{j},\sigma'\gamma'}^* \langle \hat{c}_{\mathbf{i},\gamma} \hat{c}_{\mathbf{j},\gamma'}^+ \rangle_0 \right. \\ \left. q_{\mathbf{i},\sigma\gamma}^* \bar{q}_{\mathbf{j},\sigma'\gamma'}^* \langle \hat{c}_{\mathbf{i},\gamma}^+ \hat{c}_{\mathbf{j},\gamma'}^+ \rangle_0 + \bar{q}_{\mathbf{i},\sigma\gamma} q_{\mathbf{j},\sigma'\gamma'} \langle \hat{c}_{\mathbf{i},\gamma} \hat{c}_{\mathbf{j},\gamma'} \rangle_0 \right] \quad (82)$$

in the limit of infinite dimensions.

Analogously, for the one-particle pairing matrix we find

$$S_{\mathbf{i},\sigma;\mathbf{j}\sigma'} = \sum_{\gamma\gamma'} \left[q_{\mathbf{i},\sigma\gamma} q_{\mathbf{j},\sigma'\gamma'} \langle \hat{c}_{\mathbf{i},\gamma} \hat{c}_{\mathbf{j},\gamma'} \rangle_0 + \bar{q}_{\mathbf{i},\sigma\gamma}^* \bar{q}_{\mathbf{j},\sigma'\gamma'}^* \langle \hat{c}_{\mathbf{i},\gamma}^+ \hat{c}_{\mathbf{j},\gamma'}^+ \rangle_0 \right. \\ \left. q_{\mathbf{i},\sigma\gamma} \bar{q}_{\mathbf{j},\sigma'\gamma'}^* \langle \hat{c}_{\mathbf{i},\gamma} \hat{c}_{\mathbf{j},\gamma'}^+ \rangle_0 + \bar{q}_{\mathbf{i},\sigma\gamma}^* q_{\mathbf{j},\sigma'\gamma'} \langle \hat{c}_{\mathbf{i},\gamma}^+ \hat{c}_{\mathbf{j},\gamma'} \rangle_0 \right] \quad (83)$$

in the limit of infinite dimensions.

6 Variational ground-state energy

In this section we specify the variational problem in the limit of high dimensions. We use translational invariance to render the problem numerically tractable.

6.1 Variational problem

The variational ground-state energy for the multi-band Hamiltonian (12) is given by

$$E^{\text{var}}(\{\lambda_{I_1, I_2|\mathbf{i}}\}, \{|\Psi_0\rangle\}) = \langle \hat{H} \rangle_{\text{G}}. \quad (84)$$

With the help of the results of Section 5, this expectation value is readily evaluated in infinite dimensions. We find

$$E^{\text{var}}(\{\lambda_{I_1, I_2|\mathbf{i}}\}, \{|\Psi_0\rangle\}) = E^{\text{kin}}(\{\lambda_{I_1, I_2|\mathbf{i}}\}, \{|\Psi_0\rangle\}) + E^{\text{at}}(\{\lambda_{I_1, I_2|\mathbf{i}}\}, \{|\Psi_0\rangle\}), \quad (85)$$

$$E^{\text{kin}}(\{\lambda_{I_1, I_2|\mathbf{i}}\}, \{|\Psi_0\rangle\}) = \sum_{\mathbf{i}, \mathbf{j}; \sigma\sigma'} \sum_{\alpha, \alpha' = +, -} t_{\mathbf{i}, \mathbf{j}}^{\alpha\alpha'; \sigma\sigma'} \langle \Psi_0 | \hat{c}_{\mathbf{i}, \sigma}^{\alpha} \hat{c}_{\mathbf{j}, \sigma'}^{\alpha'} | \Psi_0 \rangle, \quad (86)$$

$$E^{\text{at}}(\{\lambda_{I_1, I_2|\mathbf{i}}\}, \{|\Psi_0\rangle\}) = \sum_{\mathbf{i}} \sum_{I_1, I_4} \bar{U}_{I_1, I_4|\mathbf{i}} m_{I_1, I_4|\mathbf{i}}^0. \quad (87)$$

where $\bar{U}_{I_1, I_2 | i}$ is given in (70). The superscripts $\alpha, \alpha' = +/ -$ were introduced in order to distinguish creation and annihilation operators ($\hat{c}^- \equiv \hat{c}$). Mathematically, these superscripts are interpreted as real numbers, e.g., $\hat{c}^{(-\alpha)}$ is equal to \hat{c}^+ or \hat{c} when $\alpha = -$ or $\alpha = +$, respectively. For the hopping amplitudes in (86) we find

$$t_{i,j}^{+-; \sigma\sigma'} = \frac{1}{2} \sum_{\tau\tau'} \left(q_{i,\tau\sigma}^* q_{j,\tau'\sigma'} t_{i,j}^{\tau\tau'} - \bar{q}_{i,\tau\sigma}^* \bar{q}_{j,\tau'\sigma'} t_{j,i}^{\tau',\tau} \right), \quad t_{i,j}^{-+; \sigma\sigma'} = - \left(t_{i,j}^{+-; \sigma\sigma'} \right)^*, \quad (88)$$

$$t_{i,j}^{++; \sigma\sigma'} = \frac{1}{2} \sum_{\tau\tau'} \left(q_{i,\tau\sigma}^* \bar{q}_{j,\tau'\sigma'}^* t_{i,j}^{\tau\tau'} - \bar{q}_{i,\tau\sigma}^* q_{j,\tau'\sigma'}^* t_{j,i}^{\tau',\tau} \right), \quad t_{i,j}^{--; \sigma\sigma'} = - \left(t_{i,j}^{++; \sigma\sigma'} \right)^*. \quad (89)$$

The interaction energy is given in terms of the variational parameters $\lambda_{I_1, I_2 | i}$ and purely local expectation values in $|\Psi_0\rangle$. With the help of Wick's theorem these expectation values can be expressed solely in terms of the local single-particle density matrix $\tilde{C}_{\mathbf{m}}$ with entries

$$C_{\mathbf{m}, \sigma\sigma'}^{\alpha\alpha'} = \langle \hat{c}_{\mathbf{m}, \sigma}^{\alpha} \hat{c}_{\mathbf{m}, \sigma'}^{\alpha'} \rangle_0. \quad (90)$$

6.2 Minimization

6.2.1 Effective single-particle Schrödinger equation

We have to optimize the variational ground-state energy (85) with respect to all parameters $\{\lambda_{I_1, I_2 | i}\}$ and the set of all one-particle quasi-particle vacua $\{|\Psi_0\rangle\}$, whereby the equations (47)–(50) have to be obeyed. The latter may be fulfilled by fixing the parameters $\{\lambda_{I_1, I_2 | i}\}$ for $|I_1|, |I_2| \leq 1$, which are then functions of \tilde{C}_i and $\{\tilde{\lambda}_i\} \equiv \{\lambda_{I_1, I_2 | i}\}$ with $|I_1|, |I_2| \geq 2$. We introduce the tensors $\tilde{\eta}_i$ of Lagrange multipliers with entries $\eta_{i, \sigma\sigma'}^{\alpha, \alpha'}$ and the multiplier E^{SP} in order to fulfill equation (90) and to ensure the normalization of $|\Psi_0\rangle$. In addition, we fix the average number of particles $N = nL$ in $|\Psi_G\rangle$ with the help of the Lagrange multiplier Λ . Then, the variational ground-state energy E_0^{var} is given by

$$E_0^{\text{var}} = \underset{\{\tilde{\lambda}_i\}, \{\tilde{C}_i\}, \{\tilde{\eta}_i\}, \Lambda, \{|\Psi_0\rangle\}, E^{\text{SP}}}{\text{Minimum}} E_c \left(\{\tilde{\lambda}_i\}, \{\tilde{C}_i\}, \{\tilde{\eta}_i\}, \Lambda, \{|\Psi_0\rangle\}, E^{\text{SP}} \right) \quad (91)$$

$$\begin{aligned} E_c(\dots) &= E^{\text{var}} \left(\{\tilde{\lambda}_i\}, \{\tilde{C}_i\} \{|\Psi_0\rangle\} \right) - E^{\text{SP}} (\langle \Psi_0 | \Psi_0 \rangle - 1) \\ &\quad - \sum_{i, \sigma\sigma'} \sum_{\alpha, \alpha'} \left[\eta_{i, \sigma\sigma'}^{\alpha\alpha'} \left(C_{i, \sigma\sigma'}^{\alpha\alpha'} - \langle \Psi_0 | \hat{c}_{i, \sigma}^{\alpha} \hat{c}_{i, \sigma'}^{\alpha'} | \Psi_0 \rangle \right) + \text{c.c.} \right] \\ &\quad + \Lambda \left(\sum_{i, \sigma} n_{i, \sigma\sigma} \left(\{\tilde{\lambda}_i\}, \{\tilde{C}_i\} \right) - N \right). \end{aligned} \quad (92)$$

The minimization with respect to $|\Psi_0\rangle$ can be carried out explicitly and leads to the effective one-particle Schrödinger equation

$$\hat{T}^{\text{eff}} |\Psi_0\rangle = E^{\text{SP}} \left(\{\tilde{\lambda}_i\}, \{\tilde{C}_i\}, \{\tilde{\eta}_i\} \right) |\Psi_0\rangle, \quad (93)$$

$$\begin{aligned} \hat{T}^{\text{eff}} &\equiv \frac{1}{2} \sum_{i, \sigma; j, \sigma'} \sum_{\alpha\alpha'} \left[\left(t_{i,j}^{\alpha\alpha'; \sigma\sigma'} + 2\delta_{i,j} \eta_{i, \sigma\sigma'}^{\alpha\alpha'} \right) \hat{c}_{i, \sigma}^{\alpha} \hat{c}_{j, \sigma'}^{\alpha'} + \text{h.c.} \right] \\ &= T_0 + \frac{1}{2} \sum_{i, \sigma; j, \sigma'} \sum_{\alpha\alpha'} \left[\left[t_{i,j}^{\alpha\alpha'; \sigma\sigma'} + \delta_{i,j} \left(\eta_{i, \sigma\sigma'}^{\alpha\alpha'} - \eta_{i, \sigma'\sigma}^{\alpha'\alpha} \right) \right] \hat{c}_{i, \sigma}^{\alpha} \hat{c}_{j, \sigma'}^{\alpha'} + \text{h.c.} \right], \end{aligned} \quad (94)$$

where

$$T_0 = \sum_{\mathbf{i}, \sigma} \left[\left(\eta_{\mathbf{i}, \sigma\sigma}^{+-} + \eta_{\mathbf{i}, \sigma\sigma}^{-+} \right) + \text{c.c.} \right]. \quad (95)$$

We assume that the optimum wave-function $|\Psi_0\rangle$ is the ground-state of the Hamiltonian (94). In this way, $|\Psi_0\rangle$ becomes a function of $\{\tilde{\lambda}_{\mathbf{i}}\}, \{\tilde{C}_{\mathbf{i}}\}, \{\tilde{\eta}_{\mathbf{i}}\}$, and the remaining task is to find the minimum

$$E_0^{\text{var}} = \underset{\{\tilde{\lambda}_{\mathbf{i}}\}, \{\tilde{C}_{\mathbf{i}}\}, \{\tilde{\eta}_{\mathbf{i}}\}, \Lambda}{\text{Minimum}} E_c(\{\tilde{\lambda}_{\mathbf{i}}\}, \{\tilde{C}_{\mathbf{i}}\}, \{\tilde{\eta}_{\mathbf{i}}\}, \Lambda), \quad (96)$$

$$\begin{aligned} E_c(\dots) &= E^{\text{SP}}(\{\tilde{\lambda}_{\mathbf{i}}\}, \{\tilde{C}_{\mathbf{i}}\}, \{\tilde{\eta}_{\mathbf{i}}\}) + E^{\text{at}}(\{\tilde{\lambda}_{\mathbf{i}}\}, \{\tilde{C}_{\mathbf{i}}\}) \\ &\quad - \sum_{\mathbf{i}, \sigma\sigma'} \left[\sum_{\alpha\alpha'} \left(\eta_{\mathbf{i}, \sigma\sigma'}^{\alpha\alpha'} C_{\mathbf{i}, \sigma\sigma'}^{\alpha\alpha'} + \text{c.c.} \right) - \delta_{\sigma\sigma'} \Lambda \left(n_{\mathbf{i}, \sigma\sigma}(\{\tilde{\lambda}_{\mathbf{i}}\}, \{\tilde{C}_{\mathbf{i}}\}) - n \right) \right]. \end{aligned} \quad (97)$$

6.2.2 Translational invariance

To make further progress we assume translational invariance. Then, the single-particle Hamiltonian in the Bloch basis with wave vectors \mathbf{k} has the form

$$\hat{T}^{\text{eff}} = T_0 + \sum_{\mathbf{k}; \sigma\sigma'} \sum_{\alpha\alpha'} \epsilon_{\sigma\sigma'}^{\alpha\alpha'}(\mathbf{k}) \hat{c}_{(\alpha\mathbf{k}), \sigma}^{\alpha} \hat{c}_{(-\alpha'\mathbf{k}), \sigma'}^{\alpha'}, \quad (98)$$

where the coefficients

$$\begin{aligned} \epsilon_{\sigma\sigma'}^{\alpha\alpha'}(\mathbf{k}) &= \frac{1}{L} \sum_{\mathbf{i}, \mathbf{j}} e^{-i\mathbf{k}(\mathbf{j}-\mathbf{i})} \left(t_{\mathbf{i}, \mathbf{j}}^{\alpha\alpha'; \sigma\sigma'} + \frac{1}{2} \delta_{\mathbf{i}, \mathbf{j}} \left(\eta_{\sigma\sigma'}^{\alpha\alpha'} - \eta_{\sigma'\sigma}^{\alpha'\alpha} + \left[\eta_{\sigma'\sigma}^{(-\alpha')(-\alpha)} \right]^* - \left[\eta_{\sigma\sigma'}^{(-\alpha)(-\alpha')} \right]^* \right) \right) \\ &= \frac{1}{2} \sum_{\tau\tau'} Q_{\tau\tau'}^{\alpha\alpha'; \sigma\sigma'} \epsilon_{\tau\tau'}^0(\mathbf{k}) + \frac{1}{2} \left(\eta_{\sigma\sigma'}^{\alpha\alpha'} - \eta_{\sigma'\sigma}^{\alpha'\alpha} + \left[\eta_{\sigma'\sigma}^{(-\alpha')(-\alpha)} \right]^* - \left[\eta_{\sigma\sigma'}^{(-\alpha)(-\alpha')} \right]^* \right) \end{aligned} \quad (99)$$

are the elements of the matrices $\tilde{\epsilon}_{\mathbf{k}}^{\alpha\alpha'}$. In (99) we used the bare energy-band matrix (14) and introduced the coefficients

$$Q_{\tau\tau'}^{+-; \sigma\sigma'} = q_{\tau\sigma}^* q_{\tau'\sigma'} - \bar{q}_{\tau\sigma}^* \bar{q}_{\tau'\sigma'}, \quad Q_{\tau\tau'}^{-+; \sigma\sigma'} = - \left(Q_{\tau\tau'}^{+-; \sigma\sigma'} \right)^* \quad (100)$$

$$Q_{\tau\tau'}^{++; \sigma\sigma'} = q_{\tau\sigma}^* \bar{q}_{\tau'\sigma'}^* - \bar{q}_{\tau\sigma}^* q_{\tau'\sigma'}^*, \quad Q_{\tau\tau'}^{--; \sigma\sigma'} = - \left(Q_{\tau\tau'}^{++; \sigma\sigma'} \right)^*. \quad (101)$$

Let us regard the operators $\hat{c}_{\mathbf{k}, \sigma}^{\alpha}$ as elements of vectors $\hat{\mathbf{c}}_{\mathbf{k}}^{\alpha}$. Then, the effective Hamiltonian \hat{T}^{eff} can be written in terms of matrix products,

$$\hat{T}^{\text{eff}} = T_0 + \sum_{\mathbf{k}} \begin{pmatrix} \hat{\mathbf{c}}_{\mathbf{k}}^+ \\ \hat{\mathbf{c}}_{-\mathbf{k}}^- \end{pmatrix}^{\text{T}} \begin{pmatrix} \tilde{\epsilon}_{\mathbf{k}}^{+-} & \tilde{\epsilon}_{\mathbf{k}}^{++} \\ \tilde{\epsilon}_{\mathbf{k}}^{-+} & \tilde{\epsilon}_{\mathbf{k}}^{--} \end{pmatrix} \begin{pmatrix} \hat{\mathbf{c}}_{\mathbf{k}}^- \\ \hat{\mathbf{c}}_{-\mathbf{k}}^+ \end{pmatrix}. \quad (102)$$

The matrix in (102) may be diagonalized by means of a Bogoliubov transformation

$$\begin{pmatrix} \hat{\mathbf{c}}_{\mathbf{k}}^- \\ \hat{\mathbf{c}}_{-\mathbf{k}}^+ \end{pmatrix} = \begin{pmatrix} \tilde{u}_{\mathbf{k}}^{--} & \tilde{u}_{\mathbf{k}}^{-+} \\ \tilde{u}_{\mathbf{k}}^{+-} & \tilde{u}_{\mathbf{k}}^{++} \end{pmatrix} \begin{pmatrix} \hat{\mathbf{h}}_{\mathbf{k}}^- \\ \hat{\mathbf{h}}_{-\mathbf{k}}^+ \end{pmatrix}, \quad (103)$$

where we introduced new fermionic operators $\hat{\mathbf{h}}_{\mathbf{k}}^{\alpha}$ and matrices $\tilde{u}_{\mathbf{k}}^{\alpha\alpha'}$ with elements $\hat{h}_{\mathbf{k},\gamma}^{\alpha}$ and $u_{\sigma\gamma}^{\alpha\alpha'}(\mathbf{k})$, respectively. For reasons of consistency the matrices $\tilde{u}_{\mathbf{k}}^{\alpha\alpha'}$ obey the symmetries

$$\tilde{u}_{-\mathbf{k}}^{++} = (\tilde{u}_{\mathbf{k}}^{--})^* \quad , \quad \tilde{u}_{-\mathbf{k}}^{+-} = (\tilde{u}_{\mathbf{k}}^{-+})^* \quad . \quad (104)$$

The fermionic commutation rules of the new operators $\hat{\mathbf{h}}_{\mathbf{k}}^{\alpha}$ are ensured when the matrix in (103) is unitary. In (102)–(104) we have used the standard notations for the transposition \widetilde{M}^T , the complex conjugate \widetilde{M}^* , and the Hermitian conjugate \widetilde{M}^\dagger of a matrix \widetilde{M} .

After the diagonalization \hat{T}^{eff} becomes

$$\begin{aligned} \hat{T}^{\text{eff}} &= T_0 + \frac{1}{2} \sum_{\mathbf{k}} \left(E_{\mathbf{k},\gamma} \hat{h}_{\mathbf{k},\gamma}^+ \hat{h}_{\mathbf{k},\gamma} - E_{\mathbf{k},\gamma} \hat{h}_{\mathbf{k},\gamma} \hat{h}_{\mathbf{k},\gamma}^+ \right) \\ &= T_0 + E_0 + \sum_{\mathbf{k}} E_{\mathbf{k},\gamma} \hat{h}_{\mathbf{k},\gamma}^+ \hat{h}_{\mathbf{k},\gamma} \quad , \end{aligned} \quad (105)$$

where the real quantities $E_{\mathbf{k},\gamma} = \delta_{\gamma\gamma'} E_{\gamma\gamma'}(\mathbf{k})$ are the elements of the diagonal matrix

$$\tilde{E}_{\mathbf{k}} = 2 \sum_{\alpha\alpha'} \left(\tilde{u}_{\mathbf{k}}^{(-\alpha)-} \right)^\dagger \tilde{\epsilon}_{\mathbf{k}}^{\alpha\alpha'} \tilde{u}_{\mathbf{k}}^{\alpha'-} \quad , \quad (106)$$

and

$$E_0 = -\frac{1}{2} \sum_{\mathbf{k}} \text{Tr} \left(\tilde{E}_{\mathbf{k}} \right) \quad . \quad (107)$$

For the derivation of (105)–(106) we have used the following symmetries of the matrices $\tilde{\epsilon}_{\mathbf{k}}^{\alpha\alpha'}$,

$$\tilde{\epsilon}_{-\mathbf{k}}^{\alpha\alpha'} = - \left(\tilde{\epsilon}_{\mathbf{k}}^{\alpha',\alpha} \right)^T = - \left(\tilde{\epsilon}_{\mathbf{k}}^{\alpha',\alpha} \right)^* \quad (\alpha \neq \alpha') \quad , \quad (108)$$

$$\tilde{\epsilon}_{-\mathbf{k}}^{\alpha,\alpha} = - \left(\tilde{\epsilon}_{\mathbf{k}}^{\alpha,\alpha} \right)^T = - \left(\tilde{\epsilon}_{\mathbf{k}}^{\alpha,\alpha} \right)^* \quad (\alpha \neq \alpha') \quad (109)$$

which follow from (99) and

$$\epsilon_{\gamma',\gamma}^0(\mathbf{k}) = \left(\epsilon_{\gamma,\gamma'}^0(\mathbf{k}) \right)^* = \epsilon_{\gamma,\gamma'}^0(-\mathbf{k}) \quad (110)$$

which result from hermiticity of \hat{T} and the fact that our electron-transfer amplitudes are real. Note that the matrices $\tilde{u}_{\mathbf{k}}^{\alpha,\alpha'}$, $\tilde{\epsilon}_{\mathbf{k}}^{\alpha\alpha'}$, the operators $\hat{h}_{\mathbf{k},\gamma}^{\alpha}$, and the energies $E_{\mathbf{k},\gamma}$ still depend on the parameters $\tilde{\lambda}, \tilde{\eta}, \tilde{C}$. The Fermi-gas ground state of (105) is given as

$$|\Psi_0(\tilde{\lambda}, \tilde{\eta}, \tilde{C})\rangle = \prod'_{\mathbf{k},\gamma} \hat{h}_{\mathbf{k},\gamma}^+ |\text{vacuum}\rangle \quad . \quad (111)$$

Here, the prime indicates that only those single-particle states with

$$E_{\mathbf{k},\gamma}(\tilde{\lambda}, \tilde{\eta}, \tilde{C}) \leq E_F \equiv 0 \quad (112)$$

are filled and

$$E^{\text{SP}}(\tilde{\lambda}, \tilde{\eta}, \tilde{C}) = T_0(\tilde{\eta}) + E_0(\tilde{\lambda}, \tilde{\eta}, \tilde{C}) + \sum'_{\mathbf{k},\gamma} E_{\mathbf{k},\gamma}(\tilde{\lambda}, \tilde{\eta}, \tilde{C}) \quad (113)$$

is the energy of the ‘Fermi-gas’ ground state. In principle, the variational ground-state energy can now be calculated by a minimization of the energy-functional

$$E_c(\tilde{\lambda}, \tilde{C}, \tilde{\eta}, \Lambda) = E^{\text{SP}}(\tilde{\lambda}, \tilde{C}, \tilde{\eta}) + E^{\text{at}}(\tilde{\lambda}, \tilde{C}) - L \sum_{\sigma\sigma'} \sum_{\alpha\alpha'} (\eta_{\sigma\sigma'}^{\alpha\alpha'} C_{\sigma\sigma'}^{\alpha\alpha'} + \text{c.c.}) + L\Lambda \left(\sum_{\sigma} n_{\sigma\sigma}(\tilde{\lambda}, \tilde{C}) - n \right) \quad (114)$$

with respect to all parameters x_i in $\tilde{\lambda}, \tilde{C}, \tilde{\eta}, \Lambda$, i.e.,

$$E_0^{\text{var}} = E_c(\tilde{\lambda}^0, \tilde{C}^0, \tilde{\eta}^0, \Lambda^0) \quad (115)$$

where

$$\left. \frac{\partial}{\partial x_i} E_c \right|_{\{x_i\}=\{x_i^0\}} = 0. \quad (116)$$

Minimizing E_c in this straightforward way requires rather time-consuming calculations of expectation values in $|\Psi_0\rangle$ for every single variation of our parameters. Such a strategy is prohibitive, in particular due to the large number of variational parameters $\tilde{\lambda}$. Therefore, one needs to develop more sophisticated numerical strategies when our general theory is to be applied to realistic model system.

7 Landau–Gutzwiller quasi-particles

The Gutzwiller theory, as described in the previous section, is a variational approach and by itself a method to examine ground-state properties only. As shown in Refs. [31, 47], it is possible to use the approximate Gutzwiller-correlated ground state for the calculation of elementary excitations. In particular, the ‘band structure’ $E_{\mathbf{k},\gamma}$ derived in the previous section gives the variational excitation energies of Landau–Gutzwiller quasi-particles.

7.1 Definition of single-particle excitations

Originally, Gutzwiller-correlated wave functions were introduced as Fermi-liquid ground states for ordinary metals [3]. More generally, they are Fermi-liquid ground states in the sense of an adiabatic continuity to some non-interacting reference system which can be a Fermi gas, a BCS superconductor, or a band insulator. For all such cases, quasi-particle and quasi-hole states are readily identified. To this end, we define quasi-particle and quasi-hole creation operators as

$$\hat{e}_{\mathbf{p},\tau}^+ := \hat{P}_G \hat{h}_{\mathbf{p},\tau}^+ (\hat{P}_G)^{-1}, \quad (117)$$

$$\hat{v}_{\mathbf{p},\tau} := \hat{P}_G \hat{h}_{\mathbf{p},\tau} (\hat{P}_G)^{-1}. \quad (118)$$

These operators obey usual Fermi anti-commutation relations,

$$[\hat{e}_{\mathbf{p},\tau}^+, \hat{v}_{\mathbf{p}',\tau'}]_+ = \delta_{\mathbf{p},\mathbf{p}'} \delta_{\tau\tau'}, \quad (119)$$

$$[\hat{e}_{\mathbf{p},\tau}^+, \hat{e}_{\mathbf{p}',\tau'}^+]_+ = [\hat{v}_{\mathbf{p},\tau}, \hat{v}_{\mathbf{p}',\tau'}]_+ = 0, \quad (120)$$

and they create quasi-particles/quasi-holes in the variational Gutzwiller ground-state, as can be seen from

$$\hat{e}_{\mathbf{p},\tau}^+ \hat{v}_{\mathbf{p},\tau} |\Psi_G\rangle = \Theta(E_F - E_{\mathbf{p},\tau}) |\Psi_G\rangle, \quad (121)$$

$$\hat{v}_{\mathbf{p},\tau} \hat{e}_{\mathbf{p},\tau}^+ |\Psi_G\rangle = \Theta(E_{\mathbf{p},\tau} - E_F) |\Psi_G\rangle. \quad (122)$$

We define the quasi-particle or quasi-hole excitation energy as

$$E_{\pm}(\mathbf{p}, \tau) \equiv \pm \left(E_{\pm}^{\text{var}}(\mathbf{p}, \tau) - E_0^{\text{var}} \right) - \mu^{\pm} \left(N_{\pm}^{\text{var}}(\mathbf{p}, \tau) - N \right), \quad (123)$$

where the upper and lower sign corresponds to quasi-particles and quasi-holes, respectively. Here,

$$E_{\pm}^{\text{var}}(\mathbf{p}, \tau) = \frac{\langle \Psi_{G,\pm}^{(\mathbf{p},\tau)} | \hat{H} | \Psi_{G,\pm}^{(\mathbf{p},\tau)} \rangle}{\langle \Psi_{G,\pm}^{(\mathbf{p},\tau)} | \Psi_{G,\pm}^{(\mathbf{p},\tau)} \rangle}, \quad N_{\pm}^{\text{var}}(\mathbf{p}, \tau) = \frac{\langle \Psi_{G,\pm}^{(\mathbf{p},\tau)} | \hat{N} | \Psi_{G,\pm}^{(\mathbf{p},\tau)} \rangle}{\langle \Psi_{G,\pm}^{(\mathbf{p},\tau)} | \Psi_{G,\pm}^{(\mathbf{p},\tau)} \rangle} \quad (124)$$

are the expectation values of the energy and the average particle number in the quasi-particle/quasi-hole states

$$|\Psi_{G,+}^{(\mathbf{p},\tau)}\rangle \equiv \hat{e}_{\mathbf{p},\tau}^+ |\Psi_G\rangle = \hat{P}_G \hat{h}_{\mathbf{p},\tau}^+ |\Psi_0\rangle \equiv \hat{P}_G |\Psi_{0,+}^{(\mathbf{p},\tau)}\rangle, \quad (125)$$

$$|\Psi_{G,-}^{(\mathbf{p},\tau)}\rangle \equiv \hat{v}_{\mathbf{p},\tau} |\Psi_G\rangle = \hat{P}_G \hat{h}_{\mathbf{p},\tau} |\Psi_0\rangle \equiv \hat{P}_G |\Psi_{0,-}^{(\mathbf{p},\tau)}\rangle. \quad (126)$$

The one-particle state $|\Psi_0\rangle$ is defined according to (111) in terms of the operators $\hat{h}_{\mathbf{k},\gamma}^+$. Note that $|\Psi_0\rangle$ and $\hat{h}_{\mathbf{k},\gamma}^+$ have to be used with their optimum values, given by the parameters $\tilde{\lambda}^0, \tilde{\eta}^0, \tilde{C}^0, \Lambda^0$. The quasi-particle excitation energy (123) is measured from the (variational) chemical potential μ^{\pm} which describes the energy for adding a particle to the system or subtracting it, respectively,

$$\mu^{\pm} = \pm (E_0^{\text{var}}(N \pm 1) - E_0^{\text{var}}(N)). \quad (127)$$

$E_0^{\text{var}}(N)$ is the (variational) ground-state energy for a system with N electrons. For a metallic or superconducting system, $\mu^+ = \mu^- = \mu$. For an insulating system, $\Delta^{\text{var}} = \mu^+ - \mu^-$ defines the gap in our variational theory. The variational ground-state energy (115) depends on the particle density $n = N/L$ implicitly, due to the n -dependence of all parameters x_i^0 in $\tilde{\lambda}^0, \tilde{C}^0, \tilde{\eta}^0, \Lambda^0$, and, explicitly, through the term $-\Lambda n$ in (114). Therefore, μ_{\pm} is given by

$$\mu_{\pm} = \frac{1}{L} \frac{d}{dn} E_c(\{x_i^0(n)\}, n) = \frac{1}{L} \sum_{\{x_i\}} \frac{\partial E_c}{\partial x_i} \Big|_{x_i=x_i^0} \frac{dx_i^0}{dn} - \Lambda_{\pm}^0 = -\Lambda_{\pm}^0, \quad (128)$$

where we used (116) and the fact that, in an insulating system, both μ_{\pm} and Λ^0 are discontinuous as a function of n .

7.2 Quasi-particle dispersion

We write the energies E_0^{var} and $E_{\pm}^{\text{var}}(\mathbf{p}, \gamma)$ in (123) as

$$\begin{aligned} E_0^{\text{var}} &= \frac{1}{2} \sum_{\sigma\sigma', \gamma\gamma', \alpha\alpha'} Q_{\sigma\sigma'}^{\alpha\alpha'; \gamma\gamma'}(\tilde{\lambda}^0, \tilde{C}^0) K_{\sigma\sigma'}^{\alpha\alpha'; \gamma\gamma'}(\tilde{\lambda}^0, \tilde{C}^0, \tilde{\eta}^0) + E^{\text{at}}(\tilde{\lambda}^0, \tilde{C}^0), \\ E_{\pm}^{\text{var}}(\mathbf{p}, \tau) &= \frac{1}{2} \sum_{\sigma\sigma', \gamma\gamma', \alpha\alpha'} Q_{\sigma\sigma'}^{\alpha\alpha'; \gamma\gamma'}(\tilde{\lambda}^0, \tilde{C}^0 + \tilde{\Delta}_{\pm}^{\mathbf{p}, \tau}) \sum_{\mathbf{k}} \epsilon_{\sigma\sigma'}^0(\mathbf{k}) \langle \Psi_{0, \pm}^{\mathbf{p}, \tau} | \hat{c}_{(\alpha\mathbf{k}, \gamma)}^{\alpha} \hat{c}_{(-\alpha'\mathbf{k}, \gamma')}^{\alpha'} | \Psi_{0, \pm}^{\mathbf{p}, \tau} \rangle \\ &\quad + E^{\text{at}}(\tilde{\lambda}^0, \tilde{C}^0 + \tilde{\Delta}_{\pm}^{\mathbf{p}, \tau}), \end{aligned} \quad (129)$$

where

$$K_{\sigma\sigma'}^{\alpha\alpha'; \gamma\gamma'}(\tilde{\lambda}, \tilde{C}, \tilde{\eta}) = \sum_{\mathbf{k}} \epsilon_{\sigma\sigma'}^0(\mathbf{k}) \langle \hat{c}_{(\alpha\mathbf{k}, \gamma)}^{\alpha} \hat{c}_{(-\alpha'\mathbf{k}, \gamma')}^{\alpha'} \rangle_0. \quad (130)$$

The tensor $\tilde{\Delta}_{\pm}^{\mathbf{p}, \tau}$ gives the change of \tilde{C} due to the creation of a quasi-particle or a quasi-hole,

$$\tilde{\Delta}_{\pm; \gamma\gamma'}^{\alpha\alpha'}(\mathbf{p}, \tau) = \pm \left(V_{\gamma\gamma'}^{\alpha\alpha'}(\mathbf{p}, \tau) - V_{\gamma'\gamma}^{\alpha'\alpha}(\mathbf{p}, \tau) \right), \quad (131)$$

where we introduced

$$V_{\gamma\gamma'}^{\alpha\alpha'}(\mathbf{p}, \tau) = \left(u_{\gamma\tau}^{(-\alpha)-}(\mathbf{p}) \right)^* u_{\gamma'\tau}^{\alpha'-}(\mathbf{p}). \quad (132)$$

The sum over \mathbf{k} in (129) is readily evaluated,

$$\begin{aligned} \sum_{\mathbf{k}} \epsilon_{\sigma\sigma'}^0(\mathbf{k}) \langle \Psi_{0, \pm}^{\mathbf{p}, \tau} | \hat{c}_{(\alpha\mathbf{k}, \gamma)}^{\alpha} \hat{c}_{(-\alpha'\mathbf{k}, \gamma')}^{\alpha'} | \Psi_{0, \pm}^{\mathbf{p}, \tau} \rangle &= K_{\sigma\sigma'}^{\alpha\alpha'; \gamma\gamma'}(\tilde{\lambda}^0, \tilde{C}^0, \tilde{\eta}^0) \\ &\quad \pm \left(V_{\gamma\gamma'}^{\alpha\alpha'}(\mathbf{p}, \tau) \epsilon_{\sigma\sigma'}^0(\mathbf{p}) - V_{\gamma'\gamma}^{\alpha'\alpha}(\mathbf{p}, \tau) \epsilon_{\sigma'\sigma}^0(\mathbf{p}) \right). \end{aligned} \quad (133)$$

To order $(1/L)^0$ the expansion of $\delta E_{\mathbf{p}, \tau}^{\pm} \equiv 2(E_{\pm}^{\text{var}}(\mathbf{p}, \tau) - E_0^{\text{var}})$ with respect to $\tilde{\Delta}_{\pm}^{\mathbf{p}, \tau}$ yields

$$\begin{aligned} \delta E_{\mathbf{p}, \tau}^{\pm} &= \pm \sum_{\sigma\sigma', \gamma\gamma'} \sum_{\alpha\alpha'} Q_{\sigma\sigma'}^{\alpha\alpha'; \gamma\gamma'} \left(V_{\gamma\gamma'}^{\alpha\alpha'}(\mathbf{p}, \tau) \epsilon_{\sigma\sigma'}^0(\mathbf{p}) - V_{\gamma'\gamma}^{\alpha'\alpha}(\mathbf{p}, \tau) \epsilon_{\sigma'\sigma}^0(\mathbf{p}) \right) \\ &\quad + \sum_{\rho\rho', \alpha\alpha'} \left[\sum_{\sigma\sigma', \gamma\gamma'} K_{\sigma\sigma'}^{\alpha\alpha'; \gamma\gamma'} \frac{\partial Q_{\sigma\sigma'}^{\alpha\alpha'; \gamma\gamma'}}{\partial C_{\rho\rho'}^{\alpha\alpha'}} \Big|_{\tilde{C}=\tilde{C}^0} + \frac{\partial E^{\text{at}}}{\partial C_{\rho\rho'}^{\alpha\alpha'}} \Big|_{\tilde{C}=\tilde{C}^0} \right] \Delta_{\pm; \rho\rho'}^{\alpha\alpha'}(\mathbf{p}, \tau) \\ &\quad + \sum_{\rho\rho', \alpha\alpha'} \left[\sum_{\sigma\sigma', \gamma\gamma'} K_{\sigma\sigma'}^{\alpha\alpha'; \gamma\gamma'} \frac{\partial Q_{\sigma\sigma'}^{\alpha\alpha'; \gamma\gamma'}}{\partial (C_{\rho\rho'}^{\alpha\alpha'})^*} \Big|_{\tilde{C}=\tilde{C}^0} + \frac{\partial E^{\text{at}}}{\partial (C_{\rho\rho'}^{\alpha\alpha'})^*} \Big|_{\tilde{C}=\tilde{C}^0} \right] \left(\Delta_{\pm; \rho\rho'}^{\alpha\alpha'}(\mathbf{p}, \tau) \right)^*. \end{aligned} \quad (134)$$

We use

$$\begin{aligned} \pm E_{\mathbf{p}, \tau} &= \pm \frac{1}{2} \sum_{\sigma\sigma', \gamma\gamma'} \sum_{\alpha\alpha'} Q_{\sigma\sigma'}^{\alpha\alpha'; \gamma\gamma'} \left(V_{\gamma\gamma'}^{\alpha\alpha'}(\mathbf{p}, \tau) \epsilon_{\sigma\sigma'}^0(\mathbf{p}) - V_{\gamma'\gamma}^{\alpha'\alpha}(\mathbf{p}, \tau) \epsilon_{\sigma'\sigma}^0(\mathbf{p}) \right) \\ &\quad + \frac{1}{2} \sum_{\gamma\gamma', \alpha\alpha'} \left[\left((\eta_{\gamma\gamma'}^{\alpha\alpha'})^0 - (\eta_{\gamma'\gamma}^{\alpha'\alpha})^0 \right) \Delta_{\pm; \gamma\gamma'}^{\alpha\alpha'}(\mathbf{p}, \tau) + \text{c.c.} \right]. \end{aligned} \quad (135)$$

to evaluate the first line in (134). For the second and the third line we employ

$$\sum_{\sigma\sigma', \gamma\gamma'} K_{\sigma\sigma'}^{\alpha\alpha'; \gamma\gamma'} \frac{\partial Q_{\sigma\sigma'}^{\alpha\alpha'; \gamma\gamma'}}{\partial C_{\rho\rho'}^{\alpha\alpha'}} \Big|_{\tilde{C}=\tilde{C}^0} = \left\langle \frac{\partial}{\partial C_{\rho\rho'}^{\alpha\alpha'}} \hat{T}^{\text{eff}} \right\rangle_0 = \frac{\partial E^{\text{SP}}}{\partial C_{\rho\rho'}^{\alpha\alpha'}} \Big|_{\tilde{C}=\tilde{C}^0} \quad (136)$$

and the corresponding equation where $C_{\rho\rho'}^{\alpha\alpha'}$ is replaced by $(C_{\rho\rho'}^{\alpha\alpha'})^*$. In (136) we have used the fact that the dependence of $K_{\sigma\sigma'}^{\alpha\alpha';\gamma\gamma'}$ on \tilde{C} can be ignored in the derivative of E^{SP} with respect to \tilde{C} because $|\Psi_0\rangle$ is an exact eigenstate of \hat{T}^{eff} and E^{SP} is its eigenvalue. Using (114) and (116) we can rewrite this expression as

$$\left. \frac{\partial E^{\text{SP}}}{\partial C_{\rho\rho'}^{\alpha\alpha'}} \right|_{\tilde{C}=\tilde{C}^0} = - \left. \frac{\partial E^{\text{at}}}{\partial C_{\rho\rho'}^{\alpha\alpha'}} \right|_{\tilde{C}=\tilde{C}^0} + \frac{1}{2} \left(\left(\eta_{\rho\rho'}^{\alpha\alpha'} \right)^0 - \left(\eta_{\rho'\rho}^{\alpha'\alpha} \right)^0 \right) - \delta_{\rho\rho'} \Lambda_{\pm}^0 \sum_{\sigma} \left. \frac{\partial n_{\sigma\sigma}}{\partial C_{\rho\rho'}^{\alpha\alpha'}} \right|_{\tilde{C}=\tilde{C}^0}, \quad (137)$$

where, again, the same equations hold with \tilde{C} and $\tilde{\eta}$ replaced by \tilde{C}^* and $\tilde{\eta}^*$, respectively. With these results and

$$N_{\pm}^{\text{var}}(\mathbf{p}, \tau) - N = \sum_{\sigma} \left[\left. \frac{\partial n_{\sigma\sigma}}{\partial C_{\rho\rho'}^{\alpha\alpha'}} \right|_{\tilde{C}=\tilde{C}^0} \Delta_{\pm;\rho\rho'}^{\alpha\alpha'} + \text{c.c.} \right] \quad (138)$$

we find $E_{\pm}(\mathbf{p}, \gamma) = E_{\mathbf{p},\gamma}$ for the quasi-particle and quasi-hole excitation energy. This relations shows that the ‘band structure’ $E_{\mathbf{p},\tau}$ describes meaningful quasi-particle bands.

8 Outlook

Our Gutzwiller theory provides a very good description of the quasi-particle band structure of ferromagnetic nickel. We obtain the correct exchange splittings and, in particular, we reproduce the experimental Fermi-surface topology. We find the correct (111)-direction of the magnetic easy axis and the right order of magnitude of the magnetic anisotropy. Our theory even reproduces the experimentally observed change of the Fermi-surface topology when the magnetic moment is oriented along the (001) axis.

Our investigations show that SDFT should be improved along the following lines. First, it needs to incorporate an orbital dependence of the exchange-correlation potential in order to reproduce the anisotropy of the exchange splittings. It may also be used to correct the partial densities of the $3d$ and $4sp$ electrons. Second, it should allow an effective spin-orbit coupling.

Thus far, our calculations have focused on the quasi-particle band structure at zero temperature. Several extensions of the Gutzwiller theory are possible. First, as shown in [47], we can also address magnetic excitations. Therefore, Gutzwiller theory should reproduce the spin-wave spectrum of nickel. Second, we can generalize the idea of elementary excitations to transitions between atomic states which are induced by photoemission. In this way we should also be able to make contact with the experimentally observed ‘6 eV-peak’ [48].

We emphasize that our Gutzwiller theory as presented here is not limited to nickel. We may apply it equally to other transition metals and their compounds, for example NiO [49]. Our theory also covers superconducting pairing which we may apply to superconductivity in multi-band systems. The Gutzwiller approach can and will be applied to many interesting correlated-electron problems in the future.

REFERENCES

References

- [1] E.P. Wohlfarth in *Handbook of Magnetic Materials* **1**, ed. by E.P. Wohlfarth (North Holland, Amsterdam, 1980), p. 1.
- [2] J.H. van Vleck, *Rev. Mod. Phys.* **25**, 220 (1953).
- [3] M.C. Gutzwiller, *Phys. Rev. Lett.* **10**, 159 (1963).
- [4] J.P. Perdew and Y. Wang, *Phys. Rev. B* **33**, 8800 (1986); A.D. Becke, *Phys. Rev. A* **38**, 3098 (1988).
- [5] M. Ulmke, *Eur. Phys. J. B* **1**, 301 (1998); J. Wahle, N. Blümer, J. Schlipf, K. Held, and D. Vollhardt, *Phys. Rev. B* **58**, 12749 (1998).
- [6] W. Nolting, W. Borgiel, V. Dose, and Th. Fauster, *Phys. Rev. B* **40**, 5015 (1989).
- [7] L. Hedin, *Phys. Rev.* **139**, A796 (1965); F. Aryasetiawan, *Phys. Rev. B* **46**, 13051 (1992).
- [8] O.K. Andersen, O. Jepsen, and D. Glötzel in *Highlights of Condensed-Matter Theory*, ed. by F. Bassani, F. Fumi, and M. Tosi (North-Holland, Amsterdam, 1985), p. 59; W.R.L. Lambrecht and O.K. Andersen, *Phys. Rev. B* **34**, 2439 (1986); O. K. Andersen and T. Saha-Dasgupta, *Phys. Rev. B* **62**, R16219 (2000).
- [9] For an introduction to dynamical mean-field theory and its applications to real materials, see, for example, K. Held, I.A. Nekrasov, G. Keller, V. Eyert, N. Blümer, A.K. McMahan, R.T. Scalettar, T. Pruschke, V.I. Anisimov, and D. Vollhardt in *Quantum Simulations of Complex Many-Body Systems: From Theory to Algorithms*, ed. by J. Grotendorst, D. Marks, and A. Muramatsu (NIC Series Vol. **10**, 2002), p. 175.
- [10] M.B. Zöfl, Th. Pruschke, J. Keller, A.I. Poteryaev, I.A. Nekrasov, and V.I. Anisimov, *Phys. Rev. B* **61**, 12810 (2000).
- [11] A.I. Lichtenstein, M.I. Katsnelson, and G. Kotliar, *Phys. Rev. Lett.* **87**, 067205 (2001).
- [12] V.I. Anisimov, J. Zaanen, and O.K. Andersen, *Phys. Rev. B* **44**, 943 (1991).
- [13] I. Yang, S.Y. Savrasov, and G. Kotliar, *Phys. Rev. Lett.* **87**, 216405 (2001).
- [14] Y. Xie and J.A. Blackman, *Phys. Rev. B* **69**, 172407 (2004).
- [15] S. Biermann, F. Aryasetiawan, and A. Georges, *Phys. Rev. Lett.* **90**, 086402 (2003).
- [16] M. Donath, *Surf. Sci. Rep.* **20**, 251 (1994).
- [17] M.B. Stearns in *Landolt–Börnstein New Series Group III*, Vol. 19A, ed. by H.P.J. Wijn (Springer, Berlin, 1986), p. 24.

REFERENCES

- [18] A. Goldmann, W. Gudat, and O. Rader in *Landolt–Börnstein New Series Group III*, Vol. 23C2, ed. by A. Goldmann (Springer, Berlin, 1994).
- [19] D.C. Tsui, Phys. Rev. **164**, 669 (1967).
- [20] H.A. Mook, Phys. Rev. **148**, 495 (1966).
- [21] D.E. Eastman, F.J. Himpsel, and J.A. Knapp, Phys. Rev. Lett. **40**, 1514 (1978).
- [22] W. Eberhardt and E.W. Plummer, Phys. Rev. B **21**, 3245 (1980).
- [23] V.L. Moruzzi, J.F. Janak, and A.R. Williams, *Calculated Electronic Properties of Metals* (Pergamon Press, New York, 1978).
- [24] This appears to be a general problem of the underlying DFT calculation. The same problem appears for $4d$ transition metals of bcc structure: the position of the purely $5p$ -state $N_{2'}$ also appears shifted by about 0.7 eV to lower energies as compared to the DFT results, see G.W. Crabtree, D.H. Dye, D.P. Karim, D.D. Koelling, and J.B. Ketterson, Phys. Rev. Lett. **42**, 390 (1977).
- [25] M.J. Singh, J. Callaway, and C.S. Wang, Phys. Rev. B **14**, 1214 (1976).
- [26] G.H.O. Daalderop, P.J. Kelly, and M.F.H. Schuurmans, Phys. Rev. B **41**, 11919 (1990).
- [27] R. Gersdorf and G. Aubert, Physica B **95**, 135 (1978).
- [28] R. Gersdorf, Phys. Rev. Lett. **40**, 344 (1978).
- [29] J. Bünemann, W. Weber, and F. Gebhard, Phys. Rev. B **57**, 6896 (1998).
- [30] J. Bünemann, F. Gebhard, T. Ohm, R. Umstätter, S. Weiser, W. Weber, R. Claessen, D. Ehm, A. Harasawa, A. Kakizaki, A. Kimura, G. Nicolay, S. Shin, and V.N. Strocov, Europhys. Lett. **61**, 667 (2003).
- [31] J. Bünemann, F. Gebhard, and R. Thul, Phys. Rev. B **67**, 075103 (2003).
- [32] J.C. Slater and G.F. Koster, Phys. Rev. **94**, 1498 (1954).
- [33] W. Weber and L.F. Mattheiss, Phys. Rev. B **25**, 2270 (1982).
- [34] T. Ohm, S. Weiser, R. Umstätter, W. Weber, J. Bünemann, J. Low Temp. Phys. **126**, 1081 (2002).
- [35] A. Abragam and B. Bleaney, *Electron paramagnetic resonance of transition ions* (Clarendon Press, Oxford, 1970).
- [36] P. Bruno in *Magnetismus von Festkörpern und Grenzflächen* (24. IFF-Ferienkurs, Forschungszentrum Jülich GmbH, 1993), p. 24-1; P. Escudier, Ann. Phys. (Paris) **9**, 125 (1975).

REFERENCES

- [37] W. Weber et al., in preparation.
- [38] S. Sugano, Y. Tanabe, and H. Kamimura, *Multiplets of Transition-Metal Ions in Crystals* (Pure and Applied Physics **33**, Academic Press, New York, 1970).
- [39] C. Herring in *Magnetism, Vol. IV*, ed. by G. T. Rado and H. Suhl (Academic Press, New York, 1966), p. 1.
- [40] I. Schnell, G. Czucholl, and R.C. Albers, Phys. Rev. B **68**, 245102 (2003).
- [41] M.S. Hybertson, M. Schlüter, and N.E. Christensen, Phys. Rev. B **39**, 9028 (1989).
- [42] G. Vielsack and W. Weber, Phys. Rev. B **54**, 6614 (1996).
- [43] V.I. Anisimov and O. Gunnarsson, Phys. Rev. B **43**, 7570 (1991).
- [44] J. Rath and A.J. Freeman, Phys. Rev. B **11**, 2109 (1975).
- [45] K.-P. Kämper, W. Schmitt, and G. Güntherodt, Phys. Rev. B **42**, 10696 (1990).
- [46] C.S. Wang and J. Callaway, Phys. Rev. B. **15**, 298 (1977); J. Callaway in *Physics of Transition Metals 1980*, ed. by P. Rhodes (Conf. Ser. Notes **55**, Inst. of Physics, Bristol, 1981), p. 1.
- [47] J. Büneemann, J. Phys. Cond. Matt. **13**, 5327 (2001).
- [48] S. Hüfner, *Photoelectron spectroscopy*, 2nd edition (Solid-State Sciences **82**, Springer, Berlin, 1995).
- [49] S. Weiser, PhD thesis (Universität Dortmund, 2005), unpublished.